Curvature, Order, and Dynamics of Lipid Hexagonal Phases Studied by Deuterium NMR Spectroscopy†

Robin L. Thurmond,‡ Göran Lindblom,§ and Michael F. Brown*

Department of Chemistry, University of Arizona, Tucson, Arizona 85721

Received October 5, 1992; Revised Manuscript Received February 9, 1993

ABSTRACT: Solid-state deuterium (^{2}H) NMR spectroscopy enables one to study both equilibrium and dynamical properties of membrane constituents at the molecular level and can yield significant insights regarding the organization of non-bilayer lipid aggregates. We have investigated a representative unsaturated phosphatidylethanolamine, viz., 1-perdeuteriopalmitoyl-2-linoleoyl-*sn*-glycero-3-phosphoethanolamine, PLPE-d_{31}, in the lamellar, or L_α, phase and the reversed hexagonal, or H_{II}, phase. Phosphorus-31 (^{31}P) NMR studies of PLPE-d_{31} in the H_{II} phase revealed that the chemical shift anisotropy of the phosphoethanolamine head groups, $\Delta\sigma$, was scaled by the expected geometrical factor of $-1/2$ relative to the lamellar state. However, we found the occurrence of a further reduction in the ^{2}H NMR quadrupolar splittings, $\Delta\nu_Q$, of the ^{2}H-labeled palmitoyl acyl chain segments. These observations point toward the role of interfacial curvature with regard to properties of reverse hexagonal phase lipids, and indicate that the pivotal position or neutral surface of approximately constant area may lie near the glycerol or polar head group region. Variations in the acyl chain packing due to curvature of the aqueous interface yield significant differences in the segmental order profiles as determined by ^{2}H NMR spectroscopy. The latter reflect the local orientational order of the acyl chains and can be used together with simple statistical theories to extract positional or structural information. Average projected acyl chain lengths and mean interfacial or cross-sectional areas for PLPE-d_{31} in the different phases have been calculated. In addition, we describe a new means of estimating the radius of curvature of H_{II} phase lipid aggregates utilizing ^{2}H NMR spectroscopy, which is based on the *difference* between the lamellar and hexagonal phase order profiles. Here the radius of curvature, R_c, is defined as the distance from the center of the water core to the lipid/water interface, near the carbonyl segments of the acyl chains, giving R_c = 25.4–28.1 Å for PLPE-d_{31} in the H_{II} phase at 60 °C. This value is in good agreement with previous X-ray diffraction studies of 1,2-dioleoyl-*sn*-glycero-3-phosphoethanolamine (DOPE). Alternatively, the data yield for the radius of the central water core that R_w = 17.8–20.5 Å at 60 °C. The differences in geometry also lead to higher quadrupolar echo relaxation rates (R_{2e}) for the lipid acyl segments closest to the aqueous interface in the H_{II} versus the L_α phase. We propose that this enhancement is due to an additional relaxation mechanism found in the hexagonal phases, namely, translational diffusion of lipids about the cylinder axes. For comparison, the normal hexagonal (H_I) and lamellar (L_α) phases of a lyotropic system comprising perdeuterated potassium laurate were also studied. *This research indicates clearly that the packing and dynamical properties of the acyl chains of phospholipids depend on the curvature of the aqueous interface and, thus, the aggregate geometry.* The latter is related to the average shape of lipids in their respective phases and to the curvature free energy, which in the planar state may influence protein-mediated functions of membranes.

Biomembranes contain a wide variety of phospholipids, although the need for this diversity remains unclear at present. One aspect that has captured the attention of investigators is the tendency of many membrane lipids to form nonlamellar phases when isolated (Cullis & de Kruijff, 1978; Deese et al., 1981; Rilfors et al., 1984; Lindblom & Rilfors, 1989; Barry et al., 1992). Moreover, there is interest in how curvature of the lipid/water interface affects packing of the lipid acyl chains [cf. Seiter and Chan (1973), Bloom et al. (1978), Bocian and Chan (1978), Fuson and Prestegard (1983a,b), Parmar et al. (1984), Gruen (1985), Halle (1991), and Lepore et al. (1992)]. Although non-bilayer phases are largely absent from association with cellular membranes [cf. Ellena et al. (1986)], the forces yielding their formation must also exist in the lamellar state and thus are of potential biological significance. The above biophysical studies of membranes and their constituents [cf. Opella et al. (1987) and Bechinger et al. (1992)] are enhanced considerably by the correlation of structural properties with function [cf. Gibson and Brown (1993)]. On the basis of existing research, it appears that lipids which form reverse hexagonal (H_{II})[1] and cubic phases are important with regard to membrane functions carried out by proteins (Navarro et al., 1984; Jensen & Schutzbach, 1984, 1988; Wiedmann et al., 1988; Lindblom & Rilfors, 1989; Eriksson et al., 1991; Brown & Gibson, 1992; Epand, 1992; Gibson & Brown, 1991, 1993). One hypothesis is that the influences of non-bilayer-forming lipids are due to changes in average properties of the membrane as the lamellar to hexagonal phase transition is approached (Deese et al., 1981; Wiedmann et al., 1988). It has been suggested that the tendency of lipid monolayers to form curved surfaces may play an important role (Gruner, 1989; Lindblom & Rilfors, 1989).

† This research was supported by National Institutes of Health (NIH) Grants GM41413, EY03754, and RR03529 and by the American Heart Association, Hawaii affiliate.

* Author to whom correspondence should be addressed.

‡ Work based in part on a dissertation submitted in partial fullfillment of the requirements for the Ph.D. degree in Biochemistry at the University of Arizona. Present Address: Departments of Chemistry and Biology, Massachusetts Institute of Technology, Cambridge, MA 02139.

§ On sabbatical leave from the Department of Physical Chemistry, University of Umeå, S-901 87, Umeå, Sweden.

0006-2960/93/0432-5394$04.00/0

Current knowledge indicates that the molecular organization of lipid aggregates is governed by a balance of intra- and intermolecular forces involving both the polar head groups and the fatty acyl chains. When the attractive and repulsive forces acting within the head group and hydrocarbon regions of the membrane are not balanced at the same cross-sectional area, as in the case of unsaturated phosphatidylethanolamines, then a *curvature elastic stress* is present. It follows that a given monolayer tends to curl spontaneously toward the aqueous region, much like a contact lens or an excised patch of a soccer or tennis ball. We have proposed that such interfacial curvature and/or lateral stresses may influence the free energies of conformational states of membrane proteins such as rhodopsin (Wiedmann et al., 1988; Gibson & Brown, 1993). The stress within the bilayer can be formulated by (Helfrich, 1973; Anderson et al., 1989)

$$g_c = \kappa(H - H_0)^2 + \bar{\kappa}K \quad (1)$$

in which g_c represents the free energy of curvature per unit area. Here $H = (c_1 + c_2)/2$ is the mean curvature; H_0, the spontaneous curvature; c_1 and c_2, the two principal curvatures; K, the Gaussian curvature; and κ and $\bar{\kappa}$, the bending rigidity and Gaussian curvature modulus, respectively. The above expression quantifies the energetic cost of bending a surface away from its spontaneous or equilibrium curvature. If H_0 is nonzero, then the most favorable state of an individual monolayer is curved, and the bilayer couple is not at equilibrium with regard to this bending energy. Consequently, it is of interest to investigate the properties of phospholipid hexagonal phases whose radius of curvature is associated with the curvature free energy in the planar state.

The most widely used technique to date for such investigations has been low-angle X-ray diffraction (Luzzati, 1968; Tate & Gruner, 1989; Rand et al., 1990). But in the case of liquid crystalline systems such methods [cf. Shipley (1968)] do not yield directly any structural or dynamical information at the molecular level. Previously, we have shown how deuterium nuclear magnetic resonance spectroscopy, ^{2}H NMR, can be used to study the properties of a nonlamellar-forming lipid, 1-perdeuteriopalmitoyl-2-linoleoyl-*sn*-glycero-3-phosphoethanolamine, PLPE-d_{31}, at atomic-level resolution (Thurmond et al., 1990). This work has revealed that the segmental order profiles of the lipid acyl segments in the H_{II} phase are decreased relative to the lamellar phase and are accompanied by a reduction in the length of the plateau region. Similar behavior has also been seen in the case of 1-perdeuteriopalmitoyl-2-oleoyl-*sn*-glycero-3-phosphoethanolamine, POPE-d_{31} (Lafleur et al., 1990). We have now investigated the H_{II} and lamellar (L_α) phases of PLPE-d_{31} in further detail and have discovered that the ^{2}H NMR line shapes and derived order profiles vary substantially. These findings can be explained largely in terms of differences in packing of the acyl chains when going from a bilayer to a cylindrical structure. One way of interpreting such ^{2}H NMR data is in terms of the mean acyl chain length and cross-sectional area of the lipids (Schindler & Seelig, 1975; Salmon et al., 1987; DeYoung & Dill, 1988; Nagle & Wiener, 1988; Ipsen et al., 1990; Thurmond et al., 1991; Jansson et al., 1992). Here we show that the *difference* in the segmental order profiles can be used to estimate the average radius of curvature of the aqueous interface in the H_{II} phase. Moreover, ^{2}H NMR techniques provide dynamical information for lipids which is unobtainable using other methods [cf. Brown and Davis (1981), Eriksson et al. (1982, 1987), Bloom and Sternin (1987), and Halle (1987)]. Variations in the NMR relaxation behavior of the hexagonal and lamellar phases were observed which reflect changes in the geometry. Finally, the normal hexagonal, or H_I, phase of a perdeuterated potassium soap was investigated for purposes of comparison. These results yield new knowledge of the structural and dynamical properties of non-bilayer-forming lipids and are pertinent to the issue of how lipid properties affect functions carried out by membrane proteins (Lindblom et al., 1986; Wiedmann et al., 1988; Lindblom & Rilfors, 1989; Bolen & Sando, 1992; Gibson & Brown, 1991, 1993).

EXPERIMENTAL PROCEDURES

Synthesis of Fatty Acids and Phospholipids. Perdeuterated fatty acids were synthesized by passing deuterium gas over the appropriate acid, obtained from Sigma (St. Louis, MO), in the presence of a 10% palladium-on-charcoal catalyst (Aldrich, Milwaukee, WI) as described (Williams et al., 1985; Salmon et al., 1987). Acyl chain perdeuterated potassium laurate (potassium laurate-d_{23}) was prepared by dissolving the perdeuterated fatty acid in 100 mL of 100% ethanol and adding 1 equiv of KOH in 75 mL of 100% ethanol. The mixture was allowed to sit overnight and was then filtered to remove the potassium laurate-d_{23} product; the precipitate was used without further purification. We employed the procedure of Jensen & Pitas (1976) to synthesize 1,2-diperdeuteriopalmitoyl-*sn*-glycero-3-phosphocholine (DPPC-d_{62}) by acylating the cadmium chloride adduct of *sn*-glycero-3-phosphocholine with the anhydride of palmitic acid-d_{31} (Mason et al., 1981). The DPPC-d_{62} was treated with snake venom phospholipase A_2 from *Crotalus adamanteus* (E.C. 3.1.1.4) (Sigma, St. Louis, MO) to yield the lysolipid, namely, 1-perdeuteriopalmitoyl-*sn*-glycero-3-phosphocholine. This product was used to prepare 1-perdeuteriopalmitoyl-2-linoleoyl-*sn*-glycero-3-phosphocholine (PLPC-d_{31}) by acylation of the *sn*-2 position with linoleic anhydride (Mason et al., 1981) derived from linoleic acid (Nu Chek Prep, Elysian, MN). Finally, transphosphatidylation of PLPC-d_{31} using phospholipase D (from Savoy cabbage) in the presence of ethanolamine yielded the desired compound, 1-perdeuteriopalmitoyl-2-linoleoyl-*sn*-glycero-3-phosphocholine (PLPE-d_{31}) (Yang et al., 1967; Comfurius & Zwaal, 1977). Column chromatography on silica gel (Bio-Sil A; Bio-Rad, Richmond, CA) was used to purify the PLPE-d_{31} (elution system consisted of $CHCl_3$ with increasing amounts of MeOH up to 30%). The purified product yielded a single spot upon thin-layer chromatography (solvent system $CHCl_3$/MeOH/H_2O, 6:4:1) when visualized both by exposure to I_2 vapor and by spraying with 40% H_2SO_4 in ethanol followed by charring on a hot plate at 270 °C. In addition, the asymmetric mixed-chain lipids were characterized by quantifying the degree of acyl chain migration. This was accomplished by dispersing a small amount of lipid in the same buffer system used for preparing

[1] Abbreviations: DLPE, 1,2-dilauroyl-*sn*-glycero-3-phosphoethanolamine; DOPE, 1,2-dioleoyl-*sn*-glycero-3-phosphoethanolamine; DPPC-d_{62}, 1,2-diperdeuteriopalmitoyl-*sn*-glycero-3-phosphocholine; EDTA, ethylenediaminetetraacetic acid; EFG, electric field gradient; ^{2}H NMR, deuterium nuclear magnetic resonance; H_I, normal hexagonal phase; H_{II}, reverse hexagonal phase; L_α, liquid crystalline phase; MOPS, 3-(*N*-morpholino)propanesulfonic acid; ^{31}P NMR, phosphorus-31 nuclear magnetic resonance; PAS, principal axis system; PLPE-d_{31}, 1-perdeuteriopalmitoyl-2-linoleoyl-*sn*-glycero-3-phosphoethanolamine; POPE-d_{31}, 1-perdeuteriopalmitoyl-2-oleoyl-*sn*-glycero-3-phosphoethanolamine; R_c, radius of curvature of H_{II} phase cylinder at lipid/water interface; R_w, radius of H_{II} phase water core; R_2, transverse relaxation rate; R_{2e}, quadrupolar echo relaxation rate; R_{2e}^{HII}, quadrupolar echo relaxation rate for H_{II} phase; $R_{2e}^{L\alpha}$, quadrupolar echo relaxation rate for L_α phase; S_{CD}, carbon–deuterium bond order parameter; T_{2e}, quadrupolar echo relaxation time; $\Delta\nu_Q$, quadrupolar splitting; $\Delta\sigma$, chemical shift anisotropy.

the lysophosphatidylcholine and then adding rattlesnake venom [cf. Salmon et al. (1987)]. The free fatty acids derived from the *sn*-2 position were transesterified with BCl_3/MeOH; this was followed by gas–liquid chromatography and identification of the methyl esters by comparison to a series of standards (Supelco, Bellefonte, PA). In no case was the amount of acyl chain migration greater than 5%. The samples were dried under high vacuum; cyclohexane was added, and the solution was then placed in an 8-mm culture tube, after which it was lyophilized and kept under high vacuum for an additional 12 h. The sample of PLPE-d_{31} was prepared by gravimetrically adding 50 wt % buffer containing 20 mM MOPS and 1 mM EDTA in deuterium-depleted water (Aldrich, Milwaukee, WI), pH = 7.1. The culture tubes were then cut to an appropriate size; Teflon plugs were inserted and sealed with high-melting wax (Petrolite, OK) and then epoxy. The potassium laurate-d_{23} samples were prepared as described above, using the same buffer, but adjusting the water content gravimetrically to achieve the desired phase [cf. Small (1986)]. All samples were vortexed lightly (<1 min) and freeze–thawed five times to ensure homogeneity.

Deuterium NMR Spectroscopy. A General Electric (Fremont, CA) GN-300 wide-bore spectrometer was used to acquire ^2H NMR spectra at a magnetic field strength of 7.05 T (^2H frequency of 46.1 MHz). The ^2H NMR spectra were obtained using a home-built, high-power probe with a horizontal solenoidal coil of diameter 8 mm as the inductor. A high-power amplifier, Henry Radio Tempo 2006, was utilized, and the signals were accumulated with an external Nicolet 2090 digital oscilloscope. The quadrupolar echo pulse sequence, $(\pi/2)_x$–τ–$(\pi/2)_y$–τ–acquire, was employed together with appropriate phase cycling (Davis et al., 1976; Bloom et al., 1980). The $\pi/2$ pulse length was 1.8 μs, and the recycle time was 0.5 s. Two thousand transients were recorded and digitized with a dwell time of 2 μs for the lamellar liquid crystalline phase, whereas 10 000 acquisitions and a 12-μs dwell time were used for the hexagonal phase spectra. Quadrature detection was used, and care was always taken to initiate the Fourier transformation at the maximum of the quadrupolar echo. Sample temperatures were monitored before and after data acquisition with an accuracy of ±0.5 °C, using a thermistor inserted directly through the magnet bore into the glass dewar containing the radio-frequency coil. The data were then transferred to a Digital Equipment Corporation Microvax II computer for off-line processing using the program NMR1 (New Methods Research, Syracuse, NY). All ^2H NMR spectra were numerically deconvoluted, or de-Paked, to obtain subspectra corresponding to the $\theta = 0°$ orientation, where θ is the angle between the bilayer normal or, alternatively, the cylinder axis in the hexagonal phase and the main magnetic field [cf. Bloom et al. (1981) and Sternin et al. (1983)]. The ^{31}P NMR spectra were obtained with the GN-300 spectrometer operating at 122 MHz (7.05 T). A phase-cycled Hahn echo sequence (Rance & Byrd, 1983) was used with inverse-gated, high-power proton decoupling applied during the data acquisition. The time to echo was 40 μs, with a spectral width of 40 kHz, a pulse length of 22 μs (90°), and a relaxation delay of 1 s. Typically 500 to 2000 scans were accumulated and then multiplied by a decaying exponential corresponding to 100-Hz line broadening in the frequency domain to apodize the spectra.

The ^2H NMR transverse relaxation experiments employed the quadrupolar echo sequence in which the pulse delay τ was varied (Davis et al., 1976; Bloom et al., 1980). The T_{2e} values were obtained from de-Paked spectra using a nonlinear regression program to fit the intensities to a single-exponential decay, given by $S(t) = S(0)\exp(-R_{2e}t)$, where the quadrupolar echo relaxation rate $R_{2e} \equiv 1/T_{2e}$. The de-Pakeing algorithm assumes the ^2H NMR powder-type spectra are axially symmetric and scale as $P_2(\cos\theta)$, where θ is the angle between the symmetry axis (i.e., the bilayer normal in the lamellar phase and the cylinder axis in the hexagonal phases) and the static magnetic field direction, and P_2 is the second Legendre polynomial. Any dependence of the relaxation rates on orientation across the powder pattern can lead to changes in line shape as a function of the delay in the relaxation experiments. However, the various partially relaxed spectra did not yield evidence for a significant anisotropy of the transverse relaxation rates; consequently the spectral distortion upon de-Pakeing was small and was neglected as a simplifying approximation.

ANALYSIS OF EXPERIMENTAL DEUTERIUM NMR DATA

In the L_α phase the C–^2H bond segmental order parameters, $S_{CD}^{(i)}$, can be obtained directly from the quadrupolar splittings, $\Delta\nu_Q^{(i)}$, by using the relationship

$$\Delta\nu_Q^{(i)} = \frac{3}{2}\chi\left(\frac{3\cos^2\theta - 1}{2}\right)S_{CD}^{(i)} \qquad (2)$$

where the index i refers to the individual acyl chain segments. The static quadrupolar coupling constant is denoted by $\chi \equiv e^2qQ/h = 170$ kHz, in which h is Planck's constant; $\theta \equiv \beta_{DL}$ is the angle between the director axis, i.e., the bilayer normal, and the laboratory coordinate frame defined by the main magnetic field. In eq 2 the C–^2H bond segmental order parameters are given by

$$S_{CD}^{(i)} \equiv \frac{1}{2}\langle 3\cos^2\beta^{(i)} - 1\rangle \qquad (3)$$

The instantaneous angle between the ith C–^2H bond direction, i.e., the principal axis system (PAS) of the electric field gradient (EFG) tensor, and the director axis is denoted $\beta^{(i)}$ which in the lamellar phase is designated as $\beta_{PD}^{(i)}$; the brackets indicate an average over all orientations sampled on the ^2H NMR time scale. On the basis of geometrical considerations the values of $S_{CD}^{(i)}$ are presumed to be negative (Seelig, 1977). For lipids in hexagonal phases, there is an additional axis of symmetry due to translational diffusion of molecules over the surface of the cylinder. Thus another transformation of coordinates is needed to determine the order parameter, and eq 2 becomes

$$\Delta\nu_Q^{(i)} = \frac{3}{2}\chi\left(\frac{3\cos^2\theta - 1}{2}\right)\left(\frac{3\cos^2\zeta - 1}{2}\right)S_{CD}^{(i)} \qquad (4)$$

Here $\theta \equiv \beta_{CL}$ is now the angle between the cylinder axis and the laboratory coordinate frame; $\zeta \equiv \beta_{IC}$ is the angle between the internal frame (coincident with the director axis or the bilayer normal in the L_α phase) and the cylinder axis, which is assumed to be 90°; and $S_{CD}^{(i)}$ is given by eq 3 in terms of the angle $\beta^{(i)}$ between the C–^2H bond and the internal frame which in the hexagonal phases is denoted $\beta_{PI}^{(i)}$. Note that eq 4 differs from eq 2 by a geometrical factor of $P_2(\cos\zeta) \equiv (3\cos^2 90° - 1)/2 = -1/2$. *Hence the quadrupolar splittings, $\Delta\nu_Q^{(i)}$, in the hexagonal phases are scaled or reduced in absolute magnitude by a factor of 1/2 compared to the L_α phase on account of geometric considerations alone.*

It is well known that ^2H NMR spectroscopy yields information at the atomic level in the disordered liquid

crystalline phases; thus one has access to detailed information regarding their microstructure using statistical mechanical theories. In general, three levels of approximation can be distinguished. (i) First, one can consider the dimensions of the average shapes that pack within the phase of interest; details of the chain packing are largely bypassed (Luzzati, 1968; Israelachvili et al., 1976; Seelig, 1977). (ii) Second, microscopic knowledge from the ^{2}H NMR order profiles can be introduced which reveals a decrease in ordering along the chains; data for the initial segments can then be used to estimate the interfacial molecular area (Thurmond et al., 1991). (iii) Third, a detailed statistical mechanical treatment of the entire order profiles can be carried out in terms of lattice or mean-field theories (Nagle, 1975; Dill & Flory, 1980; Meraldi & Schlitter, 1981; Gruen, 1985). In this article, the data are interpreted at the first and the second of the above levels, which are illustrative of the range of the quantities derived from ^{2}H spectroscopy.

For an asymmetric, unsaturated phosphatidylethanolamine such as PLPE-d_{31}, it is assumed that properties of the phase are manifested in the data for the palmitoyl (16:0) chain at the *sn*-1 position; the *sn*-2 linoleoyl (18:2ω6) chain is presumed to behave similarly. With use of a simple diamond-lattice model (Schindler & Seelig, 1975; Salmon et al., 1987) the segmental order parameters can be related to the average length $\langle L \rangle$ traveled by the polymethylene segments relative to the all-trans state, as given by

$$\langle L \rangle = l_0\left[\left(\frac{n-m+1}{2}\right) - \sum_{i=m}^{n-1} S_{CD}^{(i)} - 3S_{CD}^{(n)}\right] \qquad (5)$$

The above formula refers to the entire acyl chain, where the characteristic 3-fold symmetry of the terminal methyl group is accounted for by the rightmost term. The index i pertains to numbering of the acyl chain, beginning with the ester carbon ($i = 1$) and ending with the methyl carbon ($i = n$); n is the number of carbon atoms ($n = 16$ for the *sn*-1 palmitoyl chain of PLPE-d_{31}, and $n = 12$ for potassium laurate-d_{23}). Alternatively, only the methylene groups in the initial part of the chain ($i < n$) can be considered (vide infra). Note that the effective acyl length is taken as extending from the C_1 carbon to the methyl carbon in the case of the *sn*-1 chain, i.e., $m = 2$, where the length of an individual carbon–carbon single bond projected onto the all-trans reference state is given by $l_0 = 1.25$ Å. Equation 5 ignores any folded-back conformations of the acyl chains [cf. Xu and Cafiso (1986) and Jonas et al. (1990)] and includes only contributions from rotational isomerization due to motions rapid on the ^{2}H NMR time scale (Salmon et al., 1987). The influences of slow motions which modulate the leftover residual ordering from faster segmental motions can likewise be considered (Brown, 1982)—these have a rather small effect on the calculated lengths and are disregarded (Jansson et al., 1992).

From the average projected chain length in the L_α phase one can then estimate the mean molecular area at the lipid/water interface; the various approaches depend on the length distribution function in the aggregates. One approximation is to consider the whole acyl chain using the above relationship, leading to (Thurmond et al., 1991)

$$\langle A \rangle = V_{chain}/\langle L \rangle \qquad (6)$$

Here V_{chain} is the chain volume (Nagle & Wilkinson, 1978; Wilkinson & Nagle, 1981; Salmon et al., 1987; Nagle & Wiener, 1988; Wiener et al., 1988), for a saturated chain given by $V_{chain} = n_{CH_2}V_{CH_2} + V_{CH_3}$, in which $V_{CH_3} \approx 2V_{CH_2}$ and $n_{CH_2} = n - m$ is the number of methylene segments used to calculate the projected chain length ($n_{CH_2} = 14$ for PLPE and 10 for potassium laurate). A second approach is to recognize that in the lamellar (L_α) phase the order profiles can be divided into two regions: the plateau region, where the segments have nearly the same order parameter, and the more disordered region corresponding to the ends of the chains (Seelig, 1977; Thurmond et al., 1991). The above is a consequence of chain-termination effects as included in more detailed lattice models of lipid bilayers [cf. Nagle (1975), Dill and Flory (1980), and Gruen (1980, 1985)]. At a certain depth in the bilayer, corresponding to the extent of the plateau region in the order profile, the influences of chain terminations become significant. Thus the chains on adjacent molecules are more disordered beyond this point to maintain the hydrocarbon density constant, which explains why the order parameters drop off so dramatically toward the chain ends. Assuming that geometrical effects can be disregarded [cf. Higgs and MacKay (1977) and Seelig (1977)], the carbon segments closest to the interface, e.g., the C_2 segment (α position), reflect most directly the surface area per molecule. In the L_α phase the C_2 segment of the *sn*-1 chain is unresolved, so that data for the plateau carbons can be used (Thurmond et al., 1991). One can then employ the volume of the plateau region of the order profile, $V_{plat} = n_{plat}V_{CH_2}$, in which n_{plat} is the number of methylene segments having volume V_{CH_2}. This yields an estimate for the average acyl chain interfacial area, denoted by $\langle A \rangle'$, given by (Jansson et al., 1992)

$$\langle A \rangle' = V_{plat}\langle 1/L \rangle_{plat} \qquad (7)$$

Note that for the plateau region use of $\langle L \rangle_{plat}^{-1}$ in place of $\langle 1/L \rangle_{plat}$ in eq 7 is clearly an approximation and yields a lower limit to the area at the interface (Jansson et al., 1992), where $\langle L \rangle_{plat}$ is calculated using eq 5 by considering only the initial part of the chain (vide supra). In the H_{II} phase there is little or no plateau region and hence no reason a priori for dividing up the order profile. Here the C_2 segment appears to be resolved so that one can use eq 7 in the limit that $n_{plat} \rightarrow 1$, yielding $\langle A \rangle' = V_{CH_2}\langle 1/L \rangle_2 \approx V_{CH_2}/\langle L \rangle_2$, i.e., the interfacial region is approximated by a cylindrical volume element where $\langle L \rangle_2 = l_0[1/2 - S_{CD}^{(2)}]$. Values estimated from ^{2}H NMR data for the interfacial or plateau segments and in the L_α phase from data for the entire chain are thus taken as lower and upper limits, respectively (Jansson et al., 1992), and are reported in the text as $\langle A \rangle'$ (or $\langle A \rangle$).

Finally, the bulk isobaric thermal expansion coefficient for the acyl chains is defined as $\alpha \equiv (1/V)(\partial V/\partial T)_P$. As discussed by Jansson et al. (1992), given the above approximations one can separate the bulk thermal expansion into coefficients parallel and perpendicular to the bilayer normal, viz., $\alpha = \alpha_\parallel + 2\alpha_\perp$, where the latter are defined as

$$\alpha_\parallel \equiv \frac{1}{\langle L \rangle}\left[\frac{\partial \langle L \rangle}{\partial T}\right]_P = \left[\frac{\partial \ln\langle L \rangle}{\partial T}\right]_P \qquad (8)$$

$$\alpha_\perp \equiv \frac{1}{2\langle A \rangle}\left[\frac{\partial \langle A \rangle}{\partial T}\right]_P = \frac{1}{2}\left[\frac{\partial \ln\langle A \rangle}{\partial T}\right]_P \qquad (9)$$

It follows that the slope of a plot of $\ln(\langle L \rangle/l_0)$ versus temperature will yield $\alpha_\parallel$, and likewise $2\alpha_\perp$ can be obtained from a plot of $\ln(\langle A \rangle'/a_0)$ or $\ln(\langle A \rangle/a_0)$ versus temperature. The values of $\langle L \rangle$ and $\langle A \rangle'$ or $\langle A \rangle$ are divided by the values of $l_0 = 1.25$ Å and $a_0 = 20.4$ Å^2, corresponding to the length and the cross-sectional area per methylene group, respectively, in which the all-trans state is taken as a reference [cf. Tardieu

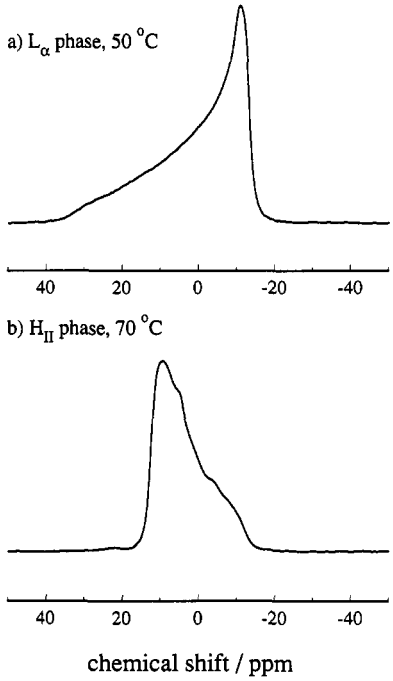

FIGURE 1: Representative proton-decoupled ^{31}P NMR spectra obtained at 122 MHz (7.05 T) of aqueous dispersions of PLPE-d_{31} containing 20 mM MOPS buffer at pH = 7.1 (50 wt % H_2O). Powder-type spectra are shown for (a) the liquid crystalline lamellar (L_α) phase at 50 °C and (b) the reverse hexagonal (H_{II}) phase at 70 °C. Note that the ^{31}P NMR chemical shift anisotropy, $\Delta\sigma$, is scaled by *approximately the expected geometrical factor of −1/2* between the two phases.

et al. (1973)]. If one assumes that the change in volume with respect with temperature is negligible as a simplifying approximation, then $\alpha_{\parallel} = -2\alpha_{\perp}$ [but see Nagle and Wilkinson (1978)].

RESULTS

Phosphorus-31 NMR Spectroscopy of an Unsaturated Phosphatidylethanolamine in the Reverse Hexagonal and Lamellar Liquid Crystalline Phases. Figure 1 shows representative phosphorus-31 (^{31}P) NMR spectra of an aqueous dispersion of 1-perdeuteriopalmitoyl-2-linoleoyl-*sn*-glycero-3-phosphocholine, PLPE-d_{31}, at temperatures of 50 and 70 °C. The observed ^{31}P NMR spectra are due to the phosphoethanolamine head groups of PLPE-d_{31}. Part a of Figure 1 shows that at 50 °C the PLPE-d_{31} dispersion yields a ^{31}P NMR spectrum characteristic of the *lamellar* (L_α) phase, with a predominant low-frequency (right) maximum and a smaller high-frequency (left) shoulder [cf. Seelig (1978) and Griffin (1981)]. As the temperature is increased to 70 °C, part b of Figure 1 indicates that a reversal in sign and a reduction in width of the ^{31}P NMR spectra occur due to formation of the *reverse hexagonal* (H_{II}) phase. The additional averaging about the cylinder axes in the H_{II} phase scales the ^{31}P NMR chemical shift anisotropy, $\Delta\sigma$, by almost exactly the geometrical factor −1/2, where $\Delta\sigma$ is equal to −40 ppm in the L_α phase and 19 ppm in the H_{II} phase. This behavior has been seen previously for other phospholipids in the reverse hexagonal phase (Cullis & de Kruijff, 1979) and suggests that the average orientations of the head groups do not vary appreciably when going from one state to the other. Such changes in head group orientation have been seen previously for a lysophospholipid, 1-palmitoyl-*sn*-glycero-3-phosphocholine, in the lamellar phase vis-à-vis the parent diacylphospholipid, 1,2-dipalmitoyl-*sn*-glycero-3-phosphocholine (Jansson et al., 1990).

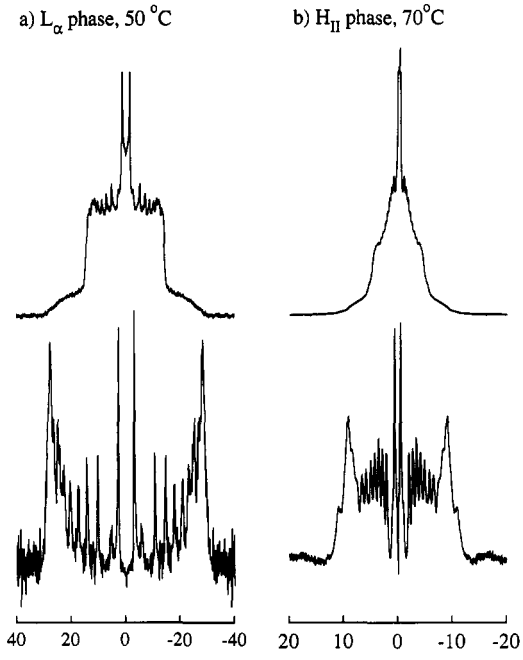

FIGURE 2: Representative ^2H NMR spectra obtained at 46.1 MHz (7.05 T) of aqueous dispersions of PLPE-d_{31} containing 20 mM MOPS buffer at pH = 7.1 (50 wt % H_2O). Powder-type spectra of random dispersions are shown at the top, and the corresponding de-Paked spectra ($\theta = 0°$) are directly beneath, for (a) the L_α phase at 50 °C and (b) the H_{II} phase at 70 °C. Here the frequency axes of the ^2H NMR spectra are different, in which the scale for the H_{II} phase is one-half that for the L_α phase. It can be seen that the widths of the H_{II} phase spectra are reduced by *more than the expected geometrical factor of 1/2* compared to the L_α phase spectra.

Deuterium NMR Spectra of the Reverse Hexagonal and Lamellar Phases of PLPE-d_{31} Reveal Differences Due to Packing of the Acyl Chains. In Figure 2 are shown ^2H NMR spectra of the unsaturated phosphatidylethanolamine PLPE-d_{31} in both the liquid crystalline lamellar (L_α) and reverse hexagonal (H_{II}) phases. The powder-type ^2H NMR spectra of the randomly oriented dispersions are shown at the top, and the corresponding de-Paked subspectra are shown at the bottom plotted on the same frequency axes. In both cases, the sharp edges of the powder-type ^2H NMR spectra correspond to the $\theta = 90°$ orientation of the symmetry axis (the bilayer normal for the L_α phase and the cylinder axis for the H_{II} phase) with respect to the main magnetic field, whereas the de-Paked subspectra reflect the $\theta = 0°$ orientation. The latter are more highly resolved because the splittings are spread out to the fullest extent possible (cf. eqs 2 and 4). The observed quadrupolar splittings arise from the perdeuterated *sn*-1 chain of PLPE-d_{31} and reveal that a profile of the segmental ordering exists along the chains. Consequently, information at the atomic level is obtained within the disordered liquid crystalline lamellar and hexagonal phase aggregates. In the L_α phase (Figure 2, part a) the segments having the largest quadrupolar splittings are nearly equivalent, with a number of additional splittings of reduced magnitude toward the spectral center. The ^2H NMR spectra of the H_{II} phase (Figure 2, part b) indicate that the residual quadrupolar couplings are all reduced substantially. Moreover, this reduction is *greater* than that expected due to the change in symmetry when going from a planar to a cylindrical geometry (cf. eq 4) in contrast to what is seen in ^{31}P NMR spectroscopy (Figure 1). Another obvious difference involves the shape of the ^2H NMR spectra. The L_α phase powder-type spectra have a "rectangular" shape,

Table I: Quadrupolar Splittings, $|\Delta\nu_Q\ (\theta = 0°)|$, and Relaxation Rates, R_{2e}, for 1-Perdeuteriopalmitoyl-2-linoleoyl-*sn*-glycero-3-phosphoethanolamine (PLPE-d_{31}) in Lamellar (L_α) and Reverse Hexagonal (H_{II}) Phases

		$\lvert\Delta\nu_Q\ (\theta = 0°)\rvert$/kHz[a]								R_{2e}/ms[b]		
		T/°C (L_α)				T/°C (H_{II})						
resonance[c]	carbon assignment	40	45	50	carbon assignment	60	70	80	90	carbon assignment	50 °C (L_α)	carbon assignment	60 °C (H_{II})
1	C_2–C_6	58.7	56.5	54.3	C_2	22.6	21.5	20.4	19.3	C_2–C_6	1890 ± 200	C_2–C_8	2670 ± 220
2	C_7	54.8	52.6	50.4	C_3–C_5	19.3	18.1	16.9	15.8	C_7	1400 ± 170	C_9	2770 ± 250
3	C_8–C_{10}	50.5	48.3	46.1	C_6–C_7	17.8	16.4	15.1	13.7	C_8–C_{10}	2630 ± 215	C_{10}	2390 ± 160
4	C_{11}	44.6	42.4	40.2	C_8	16.5	15.1	13.7	12.3	C_{11}	2850 ± 210	C_{11}	2100 ± 240
5	C_{12}	40.4	38.5	36.5	C_9	14.5	13.0	11.7	10.5	C_{12}	1540 ± 160	C_{12}	1750 ± 200
6	C_{13}	34.5	33.0	31.4	C_{10}	12.9	11.6	10.4	9.28	C_{13}	1560 ± 200	C_{13}	1730 ± 165
7	C_{14}	27.5	26.1	24.7	C_{11}	11.0	9.83	8.84	7.81	C_{14}	1450 ± 180	C_{14}	1480 ± 100
8	C_{15}	18.6	17.4	16.2	C_{12}	9.46	8.47	7.33	6.23	C_{15}	1390 ± 100	C_{15}	1420 ± 100
9	C_{16}	3.92	3.44	2.95	C_{13}	7.89	6.96	6.12	5.29	C_{16}	582 ± 50	C_{16}	757 ± 102
10					C_{14}	6.25	5.60	4.90	4.21				
11					C_{15}	4.60	4.09	3.42	2.82				
12					C_{16}	1.24	1.20	0.990	0.850				

[a] Quadrupolar splittings obtained by de-Pakeing ^{2}H NMR spectra. [b] Relaxation rates for decay of quadrupolar echo determined by de-Pakeing partially relaxed ^{2}H NMR spectra (cf. text). [c] Resonances are numbered sequentially in order of decreasing quadrupolar splitting.

apart from the smallest splitting in the center due to the terminal methyl groups (part a of Figure 2, top). This type of shape has been seen for other phosphatidylcholines and phosphatidylethanolamines in the L_α phase (Davis, 1979; Dodd, 1987; Thurmond et al., 1991) and indicates the existence of a plateau in the distribution of quadrupolar splittings as a function of segment position. The H_{II} phase powder-type spectrum (part b of Figure 2, top) has a more "triangular" appearance, which most likely reflects the smaller quadrupolar splittings in relation to the line widths, yielding greater overlap of the individual peaks. These observations are further substantiated by the de-Paked subspectra shown at the bottom of Figure 2, in which overlap of the peaks is again more pronounced in the H_{II} phase than in the L_α phase. Nonetheless, a number of distinct splittings can be resolved in both cases. The quadrupolar splittings obtained from the ^{2}H NMR spectra of the aqueous dispersions of PLPE-d_{31} in the liquid crystalline lamellar (L_α) and reverse hexagonal (H_{II}) phases are summarized for convenience in Table I.

The order parameters due to the various nonequivalent chain segments, $S_{CD}^{(i)}$, can be extracted from the splittings of the de-Paked ^{2}H NMR spectra using eqs 2 and 4. The quadrupolar splittings and the derived order parameters were assigned by assuming that they decrease in absolute magnitude along the chains, as seen for specifically deuterated phosphatidylcholines (Seelig, 1977), together with the integrated intensities of the de-Paked ^{2}H NMR spectra [cf. Williams et al. (1985)]. Figure 3 shows that the segmental ordering in the H_{II} phase is substantially less than in the L_α phase at all of the temperatures studied. This is true for all segments of the *sn*-1 palmitoyl chain, including the C_2 segment nearest the aqueous interface where the behavior might be expected to be similar. It is also evident that the order parameters decrease more uniformly down the chain for the H_{II} phase than in the L_α phase, where a distinct plateau is observed (Seelig, 1977). This same behavior has been observed for mixtures of perdeuterated tetradecanol and 1-palmitoyl-2-oleoyl-*sn*-glycero-3-phosphoethanolamine (POPE) in the H_{II} phase (Sternin et al., 1988), for POPE-d_{31} in excess water (Lafleur et al., 1990), and in our investigations of PLPE-d_{31} performed concurrently (Thurmond et al., 1990). In both the L_α and H_{II} phases the order parameters decrease with increasing temperature, where the relative change appears to be smaller in the latter case.

One can apply eq 5 together with the segmental order profiles to calculate the average length of the acyl chains projected along the bilayer normal in the L_α phase or along the perpendicular to the cylinder axis in the case of hexagonal phases. These values can then be used to estimate the average interfacial or chain cross-sectional area in both the L_α phase and the H_{II} phase. As noted above, for the L_α phase it is possible to consider the interfacial or plateau segments (eq 7) or, alternatively, the entire chain (eq 6), thereby providing lower and upper limits, respectively. The values of the projected length, $\langle L \rangle$, and the average areas, $\langle A \rangle'$ and $\langle A \rangle$, obtained for PLPE-d_{31} are plotted in Figure 4a,b as a function of temperature. The results show that the calculated lengths

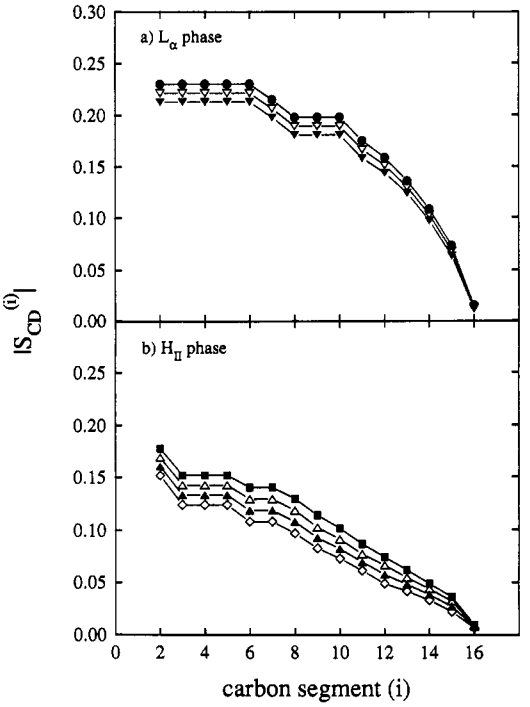

FIGURE 3: Profiles of order parameters, $|S_{CD}^{(i)}|$, derived from ^{2}H NMR quadrupolar splittings plotted versus segment position (i) at different temperatures for the *sn*-1 chain of PLPE-d_{31} in (a) the L_α phase and (b) the H_{II} phase. Experimental conditions are identical to those in the caption to Figure 2. The data were obtained at the following temperatures: 40 (●), 45 (▽), 50 (▼), 60 (■), 70 (△), 80 (▲), and 90 °C (◇). Note that the segmental order parameters in the H_{II} phase are smaller in absolute magnitude and change more gradually as a function of chain position compared to the L_α phase, where a distinct plateau is observed. The results indicate that (negative) curvature of the aqueous interface in the H_{II} phase leads to a substantial decrease in the absolute values of the order parameters versus those in the planar lamellar phase.

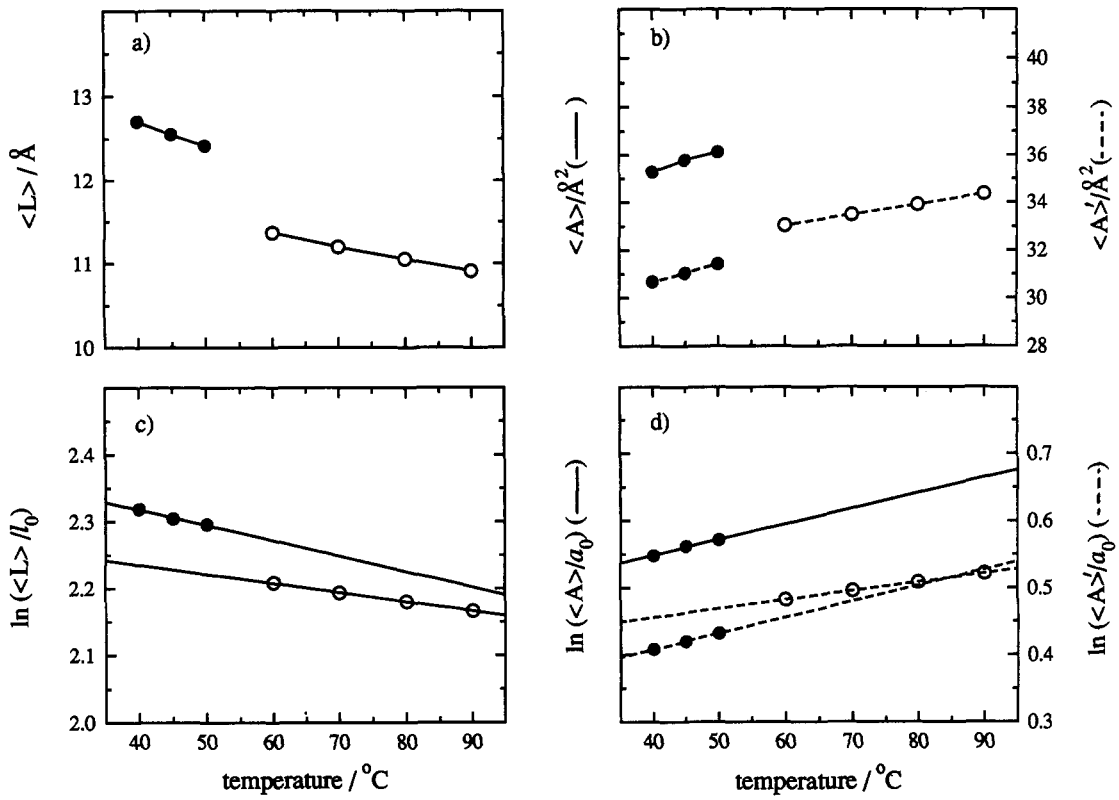

FIGURE 4: Comparison of average projected acyl lengths and cross-sectional areas for the *sn*-1 chain of PLPE-d_{31} in both the L_α phase (●) and the H_{II} phase (○). All experimental conditions are identical to those in Figure 2. The upper panels show (a) the average projected acyl length, $\langle L \rangle$, and (b) the mean interfacial or cross-sectional areas, $\langle A \rangle'$ and $\langle A \rangle$, as a function of temperature. The mean areas are estimated using ^{2}H NMR data for the interfacial or plateau segments only (- - -) and for the entire acyl chain (—) (cf. text). Note that the projected acyl chain length, $\langle L \rangle$, is *less*, and the average area, $\langle A \rangle'$, is *greater*, in the reverse hexagonal (H_{II}) phase compared to the lamellar (L_α) phase. The lower panels depict (c) the fractional changes in the average acyl chain length, $\ln(\langle L \rangle / l_0)$, and (d) the average chain areas, $\ln(\langle A \rangle'/a_0)$ and $\ln(\langle A \rangle/a_0)$, plotted versus temperature. Here the values of $\langle L \rangle$ and $\langle A \rangle'$ (or $\langle A \rangle$) are divided by their corresponding all-trans values, l_0 = 1.25 Å and a_0 = 20.4 Å^2. The slopes of the semilogarithmic plots are related to the thermal expansion coefficients for the length, $\alpha_\parallel$, and area, $\alpha_\perp$, respectively. Due to the simplifying approximation of constant total volume, the calculated changes in $\langle L \rangle$ and $\langle A \rangle'$ (or $\langle A \rangle$) are equal but opposite. In the L_α phase, the thermal expansion coefficients are $\alpha_\parallel = -2 \times 10^{-3}$ K^{-1} and $\alpha_\perp = 1 \times 10^{-3}$ K^{-1}, whereas for the H_{II} phase they are $\alpha_\parallel = -1 \times 10^{-3}$ K^{-1} and $\alpha_\perp = 5 \times 10^{-4}$ K^{-1}. The changes in the average length and area as a function of temperature are smaller for the H_{II} phase compared to the L_α phase.

are lower for the H_{II} phase, and that the areas are larger, compared to the L_α phase. For the segments closest to the aqueous interface, the estimated area value $\langle A \rangle'$ is greater in the H_{II} phase versus the L_α phase. Another important aspect is the dependence of the average projected chain lengths and the cross-sectional areas on temperature. Thermal expansion coefficients can be calculated for both the average length, $\alpha_\parallel$, and the mean cross-sectional area, $\alpha_\perp$, using eqs 8 and 9 as indicated in Figure 4c,d. Given the total volume is constant as a simplifying approximation, the expansion coefficients are roughly equal and opposite in sign for both the length and the area. For the L_α phase, $\alpha_\parallel \approx -2\alpha_\perp = -0.002$ K^{-1}, which is similar to the values obtained for a series of disaturated phosphatidylcholines using this method (Dodd, 1987). In the H_{II} phase, the expansion coefficients are smaller and are given by $\alpha_\parallel \approx -2\alpha_\perp = -0.001$ K^{-1}. These results indicate that the change in the residual ^{2}H NMR quadrupolar couplings with temperature is less for the H_{II} phase than for the L_α phase.

Deuterium NMR Spectroscopy of a Potassium Soap in the Normal Hexagonal and Lamellar Phases Evinces Further Dissimilarities. The monovalent soaps of fatty acids plus the alkali metals comprise an important class of lyotropic, liquid crystalline materials that have been studied extensively [reviewed by Ekwall (1975) and Small (1986)]. Figure 5a,b shows ^{2}H NMR spectra of potassium laurate-d_{23} in the liquid crystalline (L_α) and *normal hexagonal* (H_I) phases; the powder-type ^{2}H NMR spectra are shown at the top, and the corresponding de-Paked spectra are shown below on the same frequency axes. In the ^{2}H NMR spectrum of the L_α phase (part a of Figure 5), the quadrupolar splitting due to the C_2 segment (α position) is largest and well resolved from the remainder of the splittings, which decrease progressively along the chains [cf. Abdolall et al. (1977, 1978), Higgs and MacKay (1977), and Jeffrey et al. (1984)]. Rather similar behavior is found in the case of the H_I phase (part b of Figure 5). The splittings in the H_I phase are decreased compared to the L_α phase due to the cylindrical geometry as described above, but now the reduction is *less* than the expected factor of 1/2. This is most clearly evident from the segmental order profiles shown in Figure 5c. Here the order parameters are now somewhat greater in absolute magnitude for the H_I phase (42 wt % H_2O) compared to the L_α phase (38 wt % H_2O) at the same absolute temperature corresponding to 50 °C. Moreover, in contrast to what is seen for the L_α and H_{II} phases of PLPE-d_{31}, the order parameters of potassium laurate-d_{23} show very little change with temperature over the range 30–50 °C. At all temperatures the order parameters in the H_I phase are higher than in the L_α phase (not shown). The quadrupolar splittings obtained for the aqueous dispersions of potassium laurate-d_{23} in the lamellar (L_α) and normal hexagonal (H_I) phases are summarized in Table II. Although the C_2 position appears resolved from the rest of the chain in the case of fatty acid soaps, we have not calculated values for $\langle L \rangle$ and $\langle A \rangle'$ (or $\langle A \rangle$) due to the possibility of folding back of the chains, which complicates the interpretation of the ^{2}H NMR data.

Table II: Quadrupolar Splittings, $|\Delta\nu_Q\ (\theta = 0°)|$, and Relaxation Rates, R_{2e}, for Potassium Laurate-d_{31} in Lamellar (L_α) and Normal Hexagonal (H_I) Phases at 50 °C

		$\lvert\Delta\nu_Q\ (\theta = 0°)\rvert$/kHz[b]		R_{2e}/ms[c]	
resonance[a]	carbon assignment	38 wt % H_2O (L_α)	42 wt % H_2O (H_I)	38 wt % H_2O (L_α)	42 wt % H_2O (H_I)
1	C_2	58.6	33.7	941 ± 85	1240 ± 50
2	C_3–C_6	43.0	23.9	936 ● 30	984 ± 34
3	C_7	40.8		1110 ± 70	
4	C_8	36.6	21.0	889 ± 101	1390 ± 240
5	C_9	29.8	18.1	674 ± 74	925 ± 52
6	C_{10}	25.9	16.1	520 ± 52	725 ± 66
7	C_{11}	18.0	12.2	486 ± 60	524 ± 28
8	C_{12}	6.34	3.42	379 ± 50	346 ± 28

[a] Quadrupolar splittings obtained by de-Pakeing ^{2}H NMR spectra. [b] Relaxation rates for decay of quadrupolar echo determined by de-Pakeing partially relaxed ^{2}H NMR spectra (cf. text). [c] Resonances are numbered sequentially in order of decreasing quadrupolar splitting.

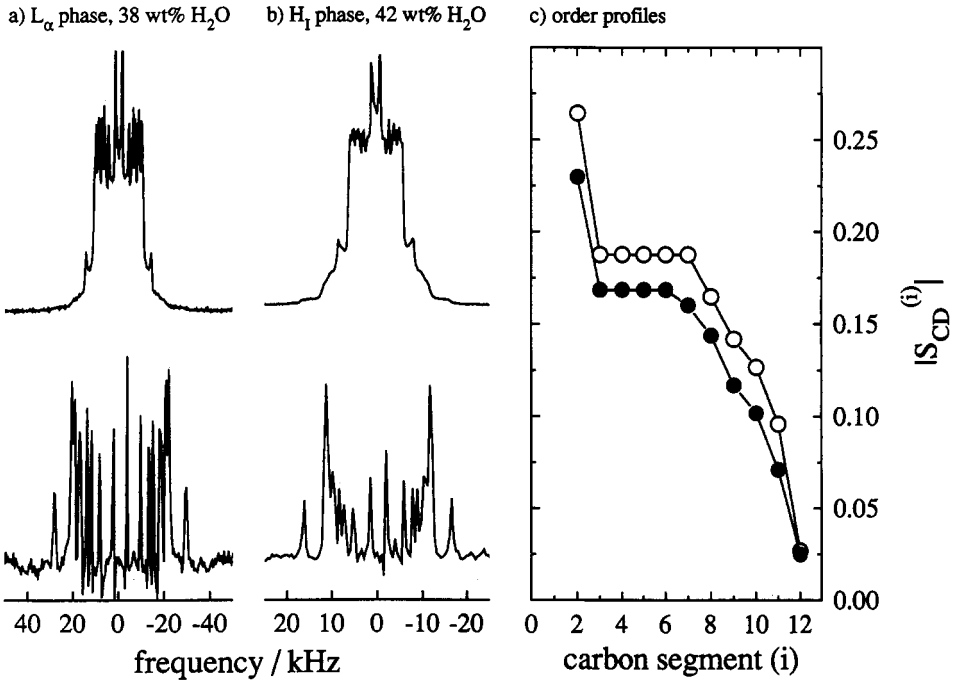

FIGURE 5: Representative ^{2}H NMR spectra and order profiles obtained at 46.1 MHz (7.05 T) for aqueous dispersions of potassium laurate-d_{23} containing 20 mM MOPS buffer at pH = 7.1. Powder-type spectra are shown at the top, and the corresponding de-Paked spectra ($\theta = 0°$) are directly beneath, for (a) the L_α phase (38 wt % H_2O) and (b) the H_I phase (42 wt % H_2O) at 50 °C. Note that the frequency scales are different for the two phases. In contrast to what is seen for the reverse hexagonal (H_{II}) phase, the ^{2}H NMR spectra for the normal hexagonal (H_I) phase are reduced by *less than the geometrical factor of 1/2* compared to the lamellar (L_α) phase. In (c) are shown segmental order profiles, $|S_{CD}^{(i)}|$, derived from the ^{2}H NMR quadrupolar splittings plotted versus chain position (i) for potassium laurate-d_{23} in the liquid crystalline lamellar (L_α) phase (●) and the normal hexagonal (H_I) phase (○) at 50 °C. The segmental order parameters in the H_I phase are larger in absolute magnitude compared to those in the L_α phase.

Deuterium NMR Relaxation Studies of Reverse Hexagonal and Normal Hexagonal Phases Indicate Variations in Dynamical Properties Compared to the Lamellar State. The transverse relaxation rates of ^{2}H nuclei in ordered media are sensitive to relatively slow motions on the NMR time scale, such as lateral diffusion of the lipids (Bloom & Sternin, 1987). Relaxation rate studies were carried out in which the decay of the quadrupolar echo was monitored as a function of the pulse delay, τ. Experimentally, the partially relaxed ^{2}H NMR spectra revealed very little orientation dependence of the transverse relaxation (not shown). This lack of a significant dependence of the relaxation on orientation across the ^{2}H NMR powder patterns is consistent with the relatively small quadrupolar splittings of the lipid hexagonal phases in relation to the spectral line widths (Figure 2). To increase the spectral resolution, the various partially relaxed spectra were de-Paked as described above. Figure 6 shows the quadrupolar echo decay rates, $R_{2e}^{(i)}$, obtained in this manner plotted aginst the chain segment position (i). In Figure 6a, the results for the reverse hexagonal and lamellar phases of PLPE-d_{31} are compared. It can be seen that the segmental relaxation rates in the plateau region are higher for the H_{II} phase compared to the L_α phase (compare data at 50 °C versus 60 °C). In the H_{II} phase the relaxation rates decrease as one moves farther down the acyl chain, whereas for the L_α phase a maximum is reached near the chain middle. Similar behavior has been seen for other phospholipids in the L_α phase (Davis, 1979, 1983; Eriksson et al., 1991). At approximately the C_8 carbon the relaxation rates become similar between the two phases. Consequently, in the H_{II} phase versus the L_α phase there is an enhancement of the relaxation corresponding to line broadening for segments in the initial part of the chain, the so-called plateau region, whereas farther down the chain the rate profiles tend to converge. For comparative purposes, Figure 6b shows plots of the $R_{2e}^{(i)}$ rates for potassium laurate-d_{23} in the normal hexagonal (H_I) phase in comparison to the lamellar (L_α) phase. Here the $R_{2e}^{(i)}$ rates are also greater than the corresponding L_α phase values, although this difference

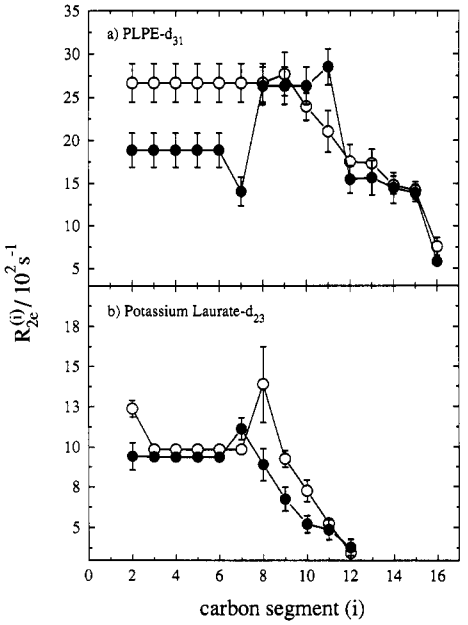

FIGURE 6: Profiles of relaxation rates for the quadrupolar echo decay, $R_{2e}^{(i)}$, as a function of chain segment position (i). The values were derived by de-Pakeing the individual partially relaxed ^2H NMR spectra (cf. text). Data are shown for (a) the *sn*-1 chain of PLPE-d_{31} in the lamellar (L_α) phase at 50 °C (●) and the reverse hexagonal (H_{II}) phase at 60 °C (○) (each containing 50 wt % H_2O) and for (b) potassium laurate-d_{23} in the lamellar (L_α) phase (38 wt % H_2O) (●) and the normal hexagonal (H_I) phase (42 wt % H_2O) (○) at 50 °C. The experimental conditions are identical to those in the captions to Figures 2 and 5. Note that the quadrupolar echo relaxation rates for the reverse hexagonal (H_{II}) phase and, to a lesser extent, the normal hexagonal (H_I) phase are larger than for the corresponding lamellar phases at similar temperatures.

is not as pronounced as for the case of the PLPE-d_{31} dispersions. The numerical values of the quadrupolar echo relaxation rates for the PLPE-d_{31} and potassium laurate-d_{23} dispersions are summarized in Tables I and II.

It should perhaps be remarked that there are several assumptions which are implicit in utilizing the de-Pakeing algorithm in relaxation studies [cf. Williams et al. (1985)]. Specifically, it is assumed that the spectral shape is invariant and scales with the orientation of the motional symmetry axis relative to the magnetic field direction as $P_2(\cos\theta)$ (Bloom et al., 1981). For random lipid dispersions, the ^2H NMR spectrum in the frequency domain is dominated by the maxima due to the $\theta = 35.3°$ and 90° orientations of the largest principal value of the electric field gradient (EFG) tensor. The smaller shoulders with twice the quadrupolar splitting correspond to the $\theta = 0°$ orientation, and the center of the spectrum with a null splitting represents the magic angle ($\theta = 54.7°$); the splittings due to the other orientations fall within these limits. The de-Paked spectrum reflects the $\theta = 0°$ orientation as a consequence of numerical evaluation using the *entire* powder-type spectrum. Consequently, the relaxation rates do not correspond to a single orientation, and thus anisotropic relaxation across the powder pattern must be negligible or nonexistent. One can expect in general that an angular anisotropy of the relaxation rates exists across the powder-type ^2H NMR spectra of random lipid dispersions [cf. Brown (1979) and Stohrer et al. (1991)]. However, the expected orientation dependence may not be detectable in powder-type lipid samples for two very different reasons. The first and most trivial cause is that contributions from the various orientations are not well resolved in the ^2H NMR spectra due to overlap of the signals. The second reason is fundamentally more interesting and was first described by Brown and Davis (1981) with regard to phospholipid lamellar phases: self-diffusion of lipids over the curved surfaces can lead to *orientational averaging* of the relaxation rates. We argue that the first case is most applicable to lipids in hexagonal phases. Although a more detailed investigation may be warranted [cf. Brown and Davis (1981)], it is doubtful that large-amplitude twisting or splaying of the hexagonally packed cylinders occurs, or that they reorient appreciably on the relatively short time scale of the transverse relaxation. The orientational anisotropy of the NMR relaxation of lipid dispersions has been the subject of a number of studies (Brown, 1979; Jarrell et al., 1988; Bonmatin et al., 1988, 1990; Speyer et al., 1989; Brown, 1990; Brown & Söderman, 1990; Mayer et al., 1990; Stohrer et al., 1991; Trouard et al., 1992).

DISCUSSION

The presence of non-bilayer-forming lipids in biological membranes has received considerable attention (Gruner, 1989; Lindblom & Rilfors, 1989; Seddon, 1990). In addition to the planar lamellar phase, phospholipids can adopt a variety of non-bilayer structures, including reversed hexagonal and cubic phases. Many of the lipids isolated from biological membrane systems tend to spontaneously form these nonlamellar phases near physiological conditions (Cullis & de Kruijff, 1979; Deese et al., 1981; Lindblom & Rilfors, 1989). Current evidence suggests that the presence of lipids which yield reverse hexagonal (H_{II}) and cubic phases are important with regard to *protein-mediated biological functions of membranes* (Navarro et al., 1984; Wiedmann et al., 1988; Lindblom & Rilfors, 1989; Eriksson et al., 1991; Brown & Gibson, 1992; Epand, 1992; Gibson & Brown, 1991, 1993). It is plausible that these effects on function reflect average properties of the membrane lipid bilayer as the lamellar to reverse hexagonal phase transition is approached (Deese et al., 1981). For a symmetric bilayer couple the two monolayers cannot simultaneously be at a free energy minimum with regard to their free energy of curvature, yielding a *condition of frustration* described by eq 1. This free energy represents a possible driving force for conformational changes of membrane proteins linked to key biological functions (Wiedmann et al., 1988; Gibson & Brown, 1993). It follows that knowledge of the equilibrium and dynamic properties of hexagonal phase lipid aggregates may be crucially important with regard to the structural biology of membrane proteins and lipids.

Effects of Interfacial Curvature on Acyl Chain Packing. Many previous experimental studies of the influences of curvature on NMR parameters related to the chain packing of lipids and amphiphiles have been carried out (Bocian & Chan, 1978; Söderman et al., 1987, 1988, 1990), and detailed theoretical models have been described (Ben-Shaul & Gelbart, 1985; Gruen, 1985; Dill et al., 1988). In most cases, amphiphiles in highly curved H_I phases or micellar aggregates as well as lipids in small unilamellar vesicles (Huang, 1969) have been compared to planar lamellar phases. The interpretation of order parameters derived from NMR relaxation studies of small vesicles in comparison to planar bilayers has a rich and colorful history (Seiter & Chan, 1973; Stockton et al., 1976; Wennerström & Lindblom, 1977; Bloom et al., 1978; Bocian & Chan, 1978; Fuson & Prestegard, 1983a,b; Kintanar et al., 1986; Korstanje et al., 1989; Halle, 1991; Lepore et al., 1992). We will not attempt to reconcile these diverse interpretations, but simply note that they tend to be model-dependent and require confirmation using an independent approach. Here we have carried out a direct ^2H NMR comparison of the influences of membrane curvature

on the packing of lipids in the reverse hexagonal (H_{II}) and lamellar phases (Figure 3). It is noteworthy that the present ^{2}H NMR line shape studies are model-free and are not complicated by aggregate reorientation or molecular diffusion, as in the case of studies of micelles and unilamellar vesicles. These ^{2}H NMR measurements clearly indicate that negative curvative of the membrane lipid/water interface leads to a decrease in the order profile relative to the lamellar phase (Lafleur et al., 1990; Thurmond et al., 1990). It follows that packing of the lipid acyl chain segments within a given monolayer is altered significantly [cf. Bocian and Chan (1978)]. Moreover, by comparing data for the lamellar and reverse haxagonal phases, one is able to estimate the radius of curvature as described below.

Interpretation of Deuterium NMR Spectra in Terms of Average Lipid Shape. Some of the differences observed in the ^{2}H NMR spectra of the hexagonal and L_α phase lipids can be explained simply in terms of the change in geometry. The first difference when going from a planar to a cylindrical geometry is an alteration of the symmetry axis along which the motions are averaged. For the L_α phase, this symmetry axis corresponds to the bilayer normal (also called the director), which can be assumed for heuristic purposes to coincide with the average orientation of the long axes of the molecules within the bilayer. In the case of hexagonal phase lipids, the molecules are oriented perpendicularly, on average, to the surface of the cylinder. The new symmetry axis arises from the additional motional averaging of the residual electric field gradient (EFG) as the molecules undergo self-diffusion over the cylindrical surface (vide supra). The diffusion is rapid on the ^{2}H NMR time scale and leads to a scaling of the residual interactions by a factor of $-1/2$ relative to the L_α phase. Moreover, because the ^{2}H NMR spectra are symmetric about the central frequency, ν_0, the change in sign is not apparent and only a reduction of the quadrupolar splitting, $\Delta\nu_Q$, is seen. Consequently, the width of the ^{2}H NMR powder patterns and the separation of the peaks in the ^{2}H NMR spectra are reduced in the reverse hexagonal (H_{II}) phase compared to the lamellar phase.

However, this is not the only change arising from the different geometry, as is evident from the ^{2}H NMR spectra of 1-perdeuteriopalmitoyl-2-linoleoyl-*sn*-glycero-3-phosphoethanolamine (PLPE-d_{31}). Even after the additional motional averaging is taken into account, the segmental order parameters, $S_{CD}^{(i)}$, are still smaller for the H_{II} phase compared to the L_α phase (Figure 3). This change is also greater than the reduction expected from the slight increase in temperature and is due to the differences in acyl chain packing between the two phases. The concept that lipids in aggregates favor certain characteristics shapes such as cones, inverted cones, and cylinders can be used to rationalize, a posteriori, which of the various phases will be formed (Tartar, 1955; Israelachvili et al., 1976; Tanford, 1980). The general idea is that the volume each lipid occupies on average must take the form of the shape which packs best into a particular phase. Lipids in a bilayer arrangement approximate the shape of a cylinder or a rectangular parallelepiped, in which the area at the lipid/water interface is nearly the same as the cross-sectional area farther down the chain. For lipids packed in the reverse hexagonal, or H_{II}, phase, however, the polar head groups are inside, and hydrocarbon chains are outside, the cylindrical aggregate. Here the lipids approximate a truncated inverted cone (geometrically a frustum), with the area at the lipid/water interface being smaller than the cross-sectional area farther down the chain. The situation in the normal hexagonal (H_I) phase is just the opposite. As mentioned above the average shape depends on the geometry of the aggregate and not the molecules themselves. Thus phosphatidylethanolamines with unsaturated acyl chains tend to form the H_{II} phase, where their average shape is that of a truncated inverted cone. Yet they also form the L_α phase, in which the average shape of the molecules approximates a cylinder or a rectangular parallelepiped. It is this difference in average shape as governed by the aggregate geometry that is reflected in the ordering of the molecules within the phase.

One quantity manifested in the average molecular shape is the area at the lipid/water interface, which in the L_α phase is related to the mean cross-sectional chain area as estimated from ^{2}H NMR spectroscopy (Thurmond et al., 1991; Jansson et al., 1992). It is generally thought that the aqueous interface is relatively broad and extends up to about the level of the C_2 or carbonyl segments of the acyl chains (Büldt et al., 1979; Wiener et al., 1991). Moreover, the ^{31}P NMR line shape is sensitive to the average orientation of the phosphate head group, so that one can use the residual ^{31}P chemical shift anisotropy, $\Delta\sigma$, to investigate whether changes in head group conformation occur in the various phases. It is noteworthy that the observed value of $\Delta\sigma$ for PLPE-d_{31} (equal to -40 ppm for the L_α phase and 19 ppm for the H_{II} phase) is scaled by nearly the expected geometrical factor of $-1/2$. This suggests that the phosphodiester orientation is most likely identical or nearly so in the two phases, and consequently it is plausible that the cross-sectional areas at the level of the head groups may be similar. However, deeper within the lipid aggregate, at the acyl C_2 segment and beyond, the ^{2}H NMR spectra dramatically reveal that the quadrupolar splittings in the reverse hexagonal (H_{II}) phase are reduced by more than the geometrical factor of $-1/2$ compared to the lamellar (L_α) phase. It follows that the acyl chains occupy a greater cross-sectional area in the H_{II} phase compared to the L_α phase, with a systematic increase with distance away from the water core. This increase in cross-sectional area along the chains corresponds to a decrease in the segmental order parameters in the H_{II} phase relative to the L_α phase, as observed experimentally (Figure 3). The above argument is also reflected in the projected lengths and cross-sectional areas averaged over the entire acyl chain. Assuming that the head group area in the H_{II} phase is roughly the same as in the L_α phase, the projected lengths of the chains must be shorter, and hence the average cross-sectional chain area must be larger, than in the L_α phase. A somewhat different qualitative interpretation holds for lipids in the normal hexagonal (H_I) phase. Here the molecules adopt a cone-like average shape, in which the cross-sectional area at the lipid/water interface is larger than near the ends of the chains on average. As a consequence, the chains are more restricted than in the L_α phase, yielding an increase in the segmental order parameters as observed experimentally (Figure 5).

These differences in geometry are also reflected in the temperature dependence of the observed ^{2}H NMR parameters. In the L_α phase, as the temperature is increased, the acyl chains of the membrane lipids become more disordered, resulting in a shortening of their projected lengths along the bilayer normal (director axis) together with an increase in cross-sectional area [cf. Meraldi and Schlitter (1981) and Gruen (1985)]. Previous work has shown that the ^{2}H NMR order profiles of membrane lipids in the L_α phase tend to fall off more gradually as a function of chain position at higher temperatures or if the lipids possess bulky polyunsaturated chains (Salmon et al., 1987). The opposite behavior is observed

in the case of phosphatidylethanolamines as compared to phosphatidylcholines in the L_α phase: the smaller cross-sectional area per molecule yields an increase in the order parameters and the length of the plateau region of the order profiles (Thurmond et al., 1991). Now in the case of PLPE-d_{31}, which has both phosphoethanolamine head groups and unsaturated chains, in the L_α phase both influences appear to be evident and thus the order parameters resemble those of other phospholipids (Figure 3). At high temperatures the reverse hexagonal (H_{II}) phase of PLPE-d_{31} is formed, in which the cross-sectional area at the aqueous interface is less than farther down the chains, yielding a characteristic ^2H NMR order profile as illustrated by Figure 3. Here the forces are balanced within the head group region at a smaller equilibrium cross-sectional area compared to the hydrocarbon tails, leading to formation of a concave aqueous interface. Nonetheless, the curvature energy is not the only factor involved. Due to the hexagonal packing of the cylinders, the average distance that a chain must traverse to fill in the hydrocarbon region, i.e., to maintain the hydrocarbon density constant, is not as uniform as in the L_α phase (Kirk et al., 1984; Sjölund et al., 1987; Gruner, 1989; Rand et al., 1990). This chain-packing energy competes with the interfacial curvature (frustration) and is one factor stabilizing the lamellar phase at sufficiently low temperatures. One can anticipate that the change in *average* projected length with temperature, as described by the thermal expansion coefficient $\alpha_\parallel$, may be smaller for the H_{II} phase than for the L_α phase as observed experimentally. Moreover, the change in temperature has an additional effect in the H_{II} phase, which may represent a continuation of the behavior in the planar L_α phase. Experimentally it is found that in the H_{II} phase the curvature of the lipid/water interface becomes greater as the chains are more disordered by a rise in temperature (Tate & Gruner, 1989). The radius of the central water core, R_w, thus becomes smaller due to the larger rate of thermal expansion within the hydrocarbon region compared to the head groups and the aqueous interface. However, the effects may be rather small, with R_w changing by only $\approx$–0.05 Å/°C over the range 60–90 °C in the case of 1,2-dioleoyl-*sn*-glycero-3-phosphoethanolamine (DOPE), and thus the differential expansion may not be detectable with ^2H NMR spectroscopy. These geometric constraints are not present in the normal hexagonal (H_I) phase, and here one expects a similar temperature dependence as in the L_α phase (e.g., for potassium laurate-d_{23} there is very little change with temperature in both phases). We shall now address the central question of whether these observations can be placed on a more quantitative footing.

Correspondence of Deuterium NMR Order Parameters to Radius of Curvature of Hexagonal Phase Cylinders. Because the order parameters of the hexagonal and L_α phases reflect packing of the acyl chains, they can be utilized to determine some of their structural features. In what follows, our attention will be confined mainly to the reverse hexagonal (H_{II}) phase in comparison to the lamellar state. We shall approximate the average shape of a lipid in the H_{II} phase as a *frustum of a right circular cone*, as depicted schematically in Figure 7. Now a decision has to be made as to where the cross-sectional areas are equivalent in the two phases, that is to say, the location of the pivotal position or the neutral surface. We have shown above that the ^{31}P NMR chemical shift anisotropy, $\Delta\sigma$, of PLPE-d_{31} in the H_{II} phase is scaled by nearly the expected geometrical factor of $-1/2$ versus the L_α phase. By contrast, the ^2H NMR quadrupolar splittings of the acyl chains beginning with the C_2 segment (α position) and beyond are

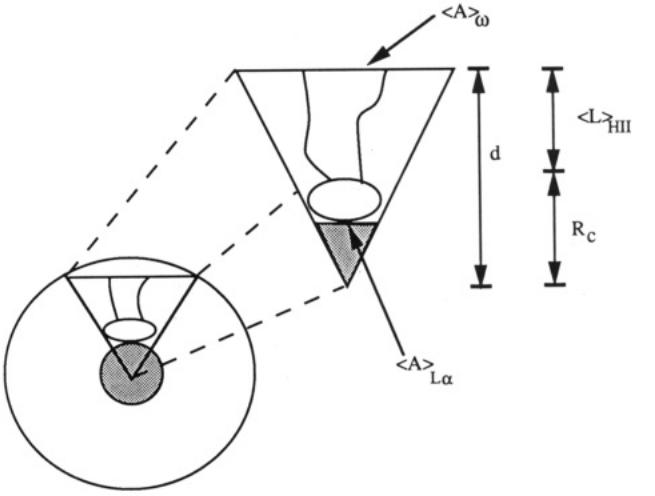

FIGURE 7: Cross-section of the reverse hexagonal (H_{II}) phase in which the average lipid shape corresponds to a frustum of a right circular cone. The shaded center indicates the water core surrounded by the polar head groups and the lipid hydrocarbon chains. Here the radius of curvature, R_c, is defined as the distance from the aqueous interface (near the carbonyl carbons of the acyl chains) to the center of the water core. The average projected chain length is denoted by $\langle L\rangle_{HII}$, and the cross-sectional areas at the lipid/water interface and at the end of the acyl chains are designated by $\langle A\rangle_{L\alpha}$ and $\langle A\rangle_\omega$, respectively. Using simple geometrical relationships, one can solve for the area of the largest base of the frustum and thereby obtain the radius of curvature, R_c (see text).

reduced by more than the factor of $-1/2$ due to the geometry alone. Hence we suggest that the areas are similar or identical at the level of the glycerol or phosphodiester moieties in the reverse hexagonal and lamellar phases. As discussed below, this is consistent with a progressive increase in cross-sectional area along the chains within the H_{II} phase aggregates, as indicated by the experimental order profiles (Figure 3).

The average cross-sectional area of the head groups $\langle A\rangle_{L\alpha}$ can be estimated from the ^2H NMR order profile of the *sn*-1 chain of PLPE-d_{31} in the planar L_α phase (Thurmond et al., 1991). Here we use two methods for estimating the interfacial or cross-sectional area in the L_α phase, and both are considered in all calculations; values are given using data for the plateau region only and, in parentheses, for the whole chain. The entire lipid is considered in calculating the dimensions of the H_{II} phase aggregates, where it is assumed for simplicity that the average length of the linoleoyl (18:2ω6) chain at the *sn*-2 position is comparable to the *sn*-1 palmitoyl (16:0) chain. Figure 7 indicates that the total length of the lipid, $\langle L\rangle_{tot}$, can be estimated as the sum of $\langle L\rangle_{HII}$ as determined from the ^2H NMR order profile of the acyl chains *in the H_{II} phase* and the projected length of the glycerophosphoethanolamine group, $\langle L\rangle_{head}$ (Nagle & Wiener, 1988). *Thus knowledge of the ^2H NMR order profiles in both the H_{II} and L_α phases is utilized.* For the H_{II} phase, the smallest cross-sectional area of the frustum is taken as that of the phosphoethanolamine head groups, whereas the largest cross-sectional area, $\langle A\rangle_\omega$, corresponds to the hydrocarbon tails. Use of simple geometrical relationships then enables one to calculate $\langle A\rangle_\omega$ by the equation

$$\langle V\rangle_{tot} = \frac{1}{3}\langle L\rangle_{tot}[\langle A\rangle_\omega + \langle A\rangle_{L\alpha} + (\langle A\rangle_{L\alpha}\langle A\rangle_\omega)^{1/2}] \qquad (10)$$

The molecular volume of PLPE-d_{31} can be obtained from dilatometry measurements and X-ray studies (Rossini et al., 1953; Tardieu et al., 1973; Nagle & Wilkinson, 1978; Wilkinson & Nagle, 1981; Nagle & Wiener, 1988; Wiener et al., 1988). The acyl chain volume is estimated from those

of the individual segments, viz., V_{CH_2} = 28.0 Å^3, V_{CH} = 20.5 Å^3, and $V_{CH_3} \approx 2V_{CH_2}$ = 56.0 Å^3. Likewise, the volume of the glycerophosphoethanolamine moiety plus the carboxyl groups is given by V_{head} = 252 Å^3 [cf. Nagle and Wiener (1988)]. We calculate for PLPE-d_{31} in the H_{II} phase that the total molecular volume including the water of hydration is $V_{tot} = V_{head} + 26V_{CH_2} + 4V_{CH} + 2V_{CH_3} + 4.7V_{H_2O}$ = (1174 + 85) = 1259 Å^3. The total projected *molecular* length is $\langle L\rangle_{tot} = \langle L\rangle_{HII} + \langle L\rangle_{head}$ = 11.3 + 7.6 = 18.9 Å, and the cross-sectional area from the ^{2}H NMR data in the planar L_α phase at 50 °C is $\langle A\rangle_{L\alpha}$ = 62.8 (72.2) Å^2. Solving for $\langle A\rangle_\omega$ in the above equation with use of the quadratic formula gives two values, 70.5 (61.2) Å^2 and 266 (266) Å^2. Because a frustum of a right circular cone is *assumed*, we consider only the negative root, and thus take the larger value of 266 Å^2 for $\langle A\rangle_\omega$. One can then use the areas of the top and bottom bases of the *frustum* to calculate the height of the corresponding *right circular cone* (in analogy to similar triangles). The equation we use for this is

$$(\langle A\rangle_{L\alpha}/\langle A\rangle_\omega)^{1/2} = (d - \langle L\rangle_{tot})/d \qquad (11)$$

where d is the cone height as depicted in Figure 7. From the above results one obtains d = 36.7 (39.4) Å, which corresponds to the radius at the ends of the acyl chains. Here we define the radius of curvature of the H_{II} phase aggregate, R_c, as the *distance from the center of the water core to the lipid/water interface*. The latter is most likely near the vicinity of the carbonyl carbons of the acyl chains, as most clearly evinced by neutron diffraction studies (Büldt et al., 1979; Wiener et al., 1991; Wiener & White, 1992). Subtraction of the projected length of the *sn*-1 acyl chain, $\langle L\rangle_{HII}$ = 11.3 Å, from the height of the right circular cone then yields R_c = 25.4 (28.1) Å as the radius of curvature of PLPE-d_{31} in the H_{II} phase at 60 °C. We have carried out the same calculations using data obtained over the temperature range 60–90 °C by substituting the corresponding values of $\langle A\rangle_{L\alpha}$ and $\langle L\rangle_{HII}$. All of these values are approximately the same, which is not surprising since X-ray data for DOPE show a relatively small change in the radius of curvature with temperature (Tate & Gruner, 1989).

One should note that the value for the projected length of the glycerophosphoethanolamine group, $\langle L\rangle_{head}$, used in these calculations is derived from an analysis of low-angle X-ray diffraction data (Nagle & Wiener, 1988). The model which seems most realistic includes bound water and gives a value for the projected length of the polar group of 1,2-dilauroyl-*sn*-glycero-3-phosphoethanolamine, DLPE, of 7.6 Å. It is tacitly assumed that the length of the glycerophosphoethanolamine moiety of PLPE-d_{31} along the normal to the interface in the H_{II} phase is the same as for DLPE in the L_α phase and that the hydration of the head groups is similar in both cases. In the alternate model (Nagle & Wiener, 1988), the polar region is considered as a laterally homogeneous strip and does not include water, yielding a projected length of $\langle L\rangle_{head}$ = 4.8 Å. If the latter value is chosen, then V_{tot} = 1174 Å^3 as indicated above, and one obtains a somewhat smaller value for the radius of curvature, R_c = 18.8 (20.7) Å. Another alternative is to assume that the neutral plane where the cross-sectional areas of the H_{II} and L_α phases are equivalent is at the level of the aqueous interface, i.e., at about the level of the carbonyl or C_2 carbons as mentioned above. Here one should recall that the ^{31}P NMR chemical shift anisotropy, $\Delta\sigma$, is scaled by the expected geometrical factor of $-1/2$ when going from the lamellar to the reverse hexagonal phase. By contrast, the ^{2}H NMR quadrupolar splittings, $\Delta\nu_Q$, of the C_2 segment and beyond are further reduced in a manner suggesting a progressive increase in cross-sectional area long the chains. In this case the results are less internally consistent (not shown) and thus support the above approach in which the length $\langle L\rangle_{head}$ is included. Assuming that the error is ±5% for all of the parameters, then the random error in R_c is ±12%, yielding R_c = 25.4 ± 3.0 (28.1 ± 3.4) Å. This estimate should be considered an upper limit, since the random errors in the various quantities are most likely less than ±5%. In addition, there are several other assumptions that will affect the calculated value for the radius of curvature. This approach ignores the curvatures at the bases of the frustum and assumes that the change in acyl chain packing when going from the hexagonal to the L_α phase occurs equally in all directions within the cylindrical surface. Both of these assumptions may lead to overestimation of the radius of curvature.

As an internal check, we can apply the same formalism to the lamellar (L_α) phase of PLPE-d_{31}. Here the total molecular volume $\langle V\rangle_{tot}$ is still 1259 Å^3, and $\langle A\rangle_{L\alpha}$ also remains the same. The total molecular length is 12.4 + 7.6 = 20.0 Å, which is only slightly larger than the value of 18.9 Å taken for the H_{II} phase. With use of eq 10, the values of $\langle A\rangle_\omega$ are now either 63.1 (54.1) Å^2 or 252 (251) Å^2. Now the positive root is chosen which corresponds to the smaller value of 63.1 (54.1) Å^2, because we *assume* the shape is a cylinder. This yields a value for the radius of curvature which is very large ($\rightarrow \infty$) as expected for a planar bilayer. Note that the former solution obtained using ^{2}H NMR data for the plateau region most closely agrees with the starting assumptions (63.1 versus 62.8 Å^2). Alternatively, one can use the smaller value for the projected head group length of $\langle L\rangle_{head}$ = 4.8 Å (Nagle & Wiener, 1988) together with $\langle V\rangle_{tot}$ = 1174 Å^3, in which case the positive root yields $\langle A\rangle_\omega$ = 73.9 (64.4) Å^2. This result is not in very good agreement with the corresponding area of 62.8 (72.2) Å estimated directly from the ^{2}H NMR data. As a further control, these numbers can be compared to the results of low-angle X-ray diffraction measurements of DOPE (Tate & Gruner, 1989; Rand et al., 1990), which are currently the most extensive data available for phospholipid reverse hexagonal phases. In order to make such a comparison, one has to be careful that the radius of curvature is defined in the same manner. In the X-ray diffraction experiments, this is defined as the maximum radius of the water cylindrical core up to the level of the lipid head groups (Gruner et al., 1986). This corresponds to subtracting the entire length of the lipid, $\langle L\rangle_{tot}$ = 18.9 Å, from the height of the cone, d, obtained from eq 11, as we have done previously (Thurmond et al., 1990).[2] We define this quantity as R_w, which in the case of DOPE is equal to 17.8 Å at 60 °C (Tate & Gruner, 1989). From the ^{2}H NMR data for PLPE-d_{31} at 60 °C we calculate that R_w = 17.8 (20.5) Å, in which the former value of 17.8 Å obtained by using only the plateau region data agrees most closely with the DOPE results. The comparison may be somewhat artificial, since PLPE-d_{31} has a much higher bilayer to hexagonal phase transition than does DOPE (55 versus 10 °C). But since the lipid structures are similar and the changes with temperature are relatively small, it is plausible that the radii of curvature are also comparable. Alternatively, one can use the smaller value of $\langle L\rangle_{head}$ = 4.8 Å, yielding R_w = 14.0 (15.9) Å. In this case the latter value of 15.9 Å obtained by using data for the entire acyl chain agrees best with the results for DOPE.

[2] The value given here differs slightly from a previous estimate (Thurmond et al., 1990) due to an error in calculating the lipid volume.

The above values are illustrative of the range of the various quantities calculated from the ^2H NMR, X-ray, and dilatometry experiments and are in fairly close agreement. Thus it appears that estimation of the radius of curvature of the H_{II} phase aggregates by ^2H NMR may provide an alternative means of obtaining this fundamentally important quantity; microscopic information at the atomic level is obtained. In passing we note that such a comparison is not possible for the case of the normal hexagonal (H_I) phase due to the greater possibility of folding back of the chains [cf. Salmon et al. (1987)]. It is known that the radii of curvature (R_c) of normal hexagonal phases (Henriksson et al., 1975) and spherical micelles (Wennerström et al., 1979; Söderman et al., 1990; Orädd et al., 1992) are close to the length of the fully extended acyl chains, which including the carboxylate is 15.8 Å in the present case.

Influences of Lipid Aggregate Geometry on Dynamical Parameters. A further advantage of ^2H NMR spectroscopy in comparison to X-ray diffraction techniques [reviewed by Shipley (1968) and Small (1986)] is that both structural and dynamical information can be obtained. As an added bonus, we now present an alternative means of estimating geometrical information for hexagonal phase aggregates based on the use of NMR relaxation methods. The problem of diffusion over a spherical surface has been considered previously (Abragam, 1961, pp 298–300; Bloom et al., 1978). Likewise self-diffusion of lipid molecules about the water core of the H_{II} phase cylinders can provide an additional relaxation mechanism in ^2H NMR spectroscopy. This can be determined by measuring the rate of decay of the quadrupolar echo, R_{2e}, which is sensitive to relatively slow motions [cf. Bloom and Sternin (1987)].

In what follows, it is assumed that the correlation times of the slow motions are less than τ, the pulse spacing in the quadrupolar echo experiment (cf. Experimental Procedures). The relaxation rate, R_{2e}, is then equal to R_2, the transverse relaxation rate [eq 139, p 315, of Abragam (1961)]. Now in ordered media the transverse relaxation rate for spin $I = 1$ nuclei is given by [Brown, 1979 (p 207), 1990]

$$R_2 = \frac{3}{8}\pi^2\chi^2[3J_0(0) + 3J_1(\omega_0) + 2J_2(2\omega_0)] \qquad (12)$$

where ω_0 is the Larmor frequency. In eq 12 the spectral density functions, $J_m(\omega)$, are defined as [cf. Abragam (1961), p 272]

$$J_m(\omega) = Re\int_{-\infty}^{\infty} G_m(t)e^{-i\omega t}\,dt \qquad (13)$$

The correlation functions, $G_m(t)$, are given by

$$G_m(t) = \frac{4\pi}{5}\langle Y_m^{(2)}(\Omega_{LP};0)Y_m^{(2)*}(\Omega_{LP};t)\rangle - |\langle KY_m^{(2)}(\Omega_{LP})\rangle|^2 \qquad (14)$$

and describe how the electric field gradient (EFG) tensor at time 0 is correlated with its orientation at time t later. Our notation is that $Y_m^{(2)}$ denotes the spherical harmonics of second rank ($m = 0, \pm1, \pm2$), and $\Omega_{LP} \equiv \Omega_{PL}^{-1}$ the (Euler) angles between the laboratory coordinate frame, defined by the main magnetic field, and the C–^2H bond direction (principal symmetry axis of EFG tensor). Note that the transverse relaxation rate, R_2, is a function of $J_0(0)$ in addition to $J_1(\omega_0)$ and $J_2(2\omega_0)$, which indicates that it depends on slow motions of the system. Further knowledge can be obtained from two-dimensional NMR (^2H or ^{31}P) exchange experiments [cf. Kaufmann et al. (1990)].

It seems reasonable to postulate that the contributions from slow motions in the L_α phase are similar in the reverse (H_{II}) and normal (H_I) hexagonal phases. Yet the hexagonal phases have an additional relaxation mechanism associated with self-diffusion of lipids around the cylinder axis. This would explain why a larger R_{2e} relaxation rate corresponding to line broadening is obtained for the reverse hexagonal (H_{II}) phase compared to the L_α phase in the plateau region of the chains (Figure 6). Thus by subtracting $R_{2e}^{L\alpha}$ from R_{2e}^{HII}, one is left with the relaxation contribution due to translational diffusion around the water cylinder, in which the separation of time scales is implicit. The difference in relaxation rates between the two phases, $R_{2e}^{HII} - R_{2e}^{L\alpha}$, corresponds to the spectral densities for diffusion around the major axis of the cylinder (cf. eq 12). For these phases, we are interested only in slow motions where $1/\tau < D_\parallel < \omega_0$, in which $D_\parallel$ is the rate of angular diffusion. Then $J_0(0)$ is the dominant contribution[3] to the excess relaxation rate, and eq 12 leads to

$$\Delta R_2 \equiv R_2^{HII} - R_2^{L\alpha} = \frac{9}{8}\pi^2\chi^2 J_0(0) \qquad (15)$$

The next step is to recognize that translational diffusion of lipids around the cylinder is formally equivalent to the problem of anisotropic rotational diffusion in the limit of complete ordering [cf. Brown (1982), section III]. Thus we only consider the limiting case where the order parameter for the restoring potential of mean torque is unity, i.e., the cylinders are rigid and not wobbling. In addition, we ignore any orientation dependence of the relaxation across the powder pattern (vide infra) and assume for simplicity that the results correspond to an orientational average, e.g., as seen in powder-type samples of multilamellar dispersions of lipids (Brown & Davis, 1981). We regard this as the less egregious of the two evils of assuming that orientational averaging occurs and considering a specific bilayer orientation, thereby contradicting the de-Pakeing algorithm. Given such a motion (cf. Appendix, eq A6), one obtains $J_m(m\omega_0) \rightarrow \langle J(m\omega_0)\rangle \equiv J(m\omega_0)$ for the orientationally averaged spectral densities, yielding

$$J(m\omega_0) = \frac{2}{5}|\langle D_{00}^{(2)}(\Omega_{PI})\rangle|^2\left[|D_{01}^{(2)}(\Omega_{IC})|^2\frac{2\tau_1^{(2)}}{1 + [m\omega_0\tau_1^{(2)}]^2} + |D_{02}^{(2)}(\Omega_{IC})|^2\frac{2\tau_2^{(2)}}{1 + [m\omega_0\tau_2^{(2)}]^2}\right] \qquad (16)$$

Here the symbols $\tau_1^{(2)}$ and $\tau_2^{(2)}$ indicate the two correlation times for the effective axial motion, and $\langle D_{00}^{(2)}(\Omega_{PI})\rangle$ is the order parameter in the H_{II} phase, also denoted by S_{CD}^{HII}, in which the segment index i is absorbed for economy of presentation (cf. eq 3). In the above equation $\Omega_{IC} = (0, \beta_{IC}, 0)$, where β_{IC} is the angle between the internal frame (local director), corresponding to the effective electric field gradient, and the symmetry axis of the cylinder. For the hexagonal phases we assume that $\beta_{IC} = 90°$, in which case $|D_{01}^{(2)}(\Omega_{IC})|^2 = 0$ and $|D_{02}^{(2)}(\Omega_{IC})|^2 = 3/8$. Inserting eq 16 for $J_0(0) \rightarrow J(0)$ into eq 15 then gives the result

$$\Delta R_2 = \frac{27}{80}\pi^2\chi^2|S_{CD}^{HII}|^2\tau_2^{(2)} \qquad (17)$$

corresponding to eq A7 (Appendix).

Let us assume that self-diffusion of lipids around the cylinder provides an additional relaxation mechanism in the H_{II} phase; then the difference in rates between the H_{II} and L_α phases reflects the radius about which this motion occurs. Because rotation of the aggregates is probably very slow and can be

[3] This assumption is only needed to simplify the algebra; otherwise all three spectral densities appear as in eq 12.

ignored, the effective correlation time, $\tau_2^{(2)}$, depends mainly on the rate of self-diffusion of lipids over the curved surface. Note that one must distinguish between the angular reorientation and the surface reorientation given in terms of the corresponding arc length. Here the rotational or *angular* diffusion coefficient $D_\parallel \rightarrow D_S/R^2$, in which D_S is the *surface* diffusion constant for motion over a cylinder of radius R. Solution of the time-dependent diffusion equation (Appendix) then yields $\tau_2^{(2)} = R^2/4D_S$, where we *assume* that D_S is the same as the *lateral* diffusion coefficient D_L in the planar L_α phase, $\approx 5 \times 10^{-12}$ m^2 s^{-1} (Lindblom et al., 1981). It follows that eq 17 becomes

$$\Delta R_2 \approx \frac{27}{320}\pi^2\chi^2|S_{CD}^{HII}|^2\frac{R^2}{D_S} \qquad (18)$$

The above formula predicts a square-law dependence of the excess relaxation rate, ΔR_2, on the hexagonal phase order parameter along the chain, analogous to the spin–lattice relaxation rate studies (R_{1Z} studies) of phospholipid lamellar phases (Brown, 1982; Williams et al., 1985). We shall mainly confine our attention to the interfacial or plateau segments for reasons that are described below. At 60 °C eq 18 can be solved to obtain the diffusion radius, R, with R_{2e}^{HII} equal to 2670 ± 221 s^{-1}, S_{CD}^{HII} equal to 0.170 for the plateau segments, and $R_{2e}^{L\alpha}$, obtained from the 50 °C measurement, equal to 1890 ± 200 s^{-1}. The value obtained for R is 23.7 Å, *assuming* that $D_S = D_L = 5 \times 10^{-12}$ m^2 s^{-1}. The propagated error in this estimate is ±5.2 Å given a 5% random error in S_{CD}^{HII} and D_L along with the errors from fitting the relaxation curves. Any differences between the values calculated here and those obtained by other methods may indicate additional contributions to the relaxation. It is noteworthy that the calculations are dependent on the value for the surface diffusion coefficient, $D_S \approx D_L$, which we can only approximate from studies of other lipids in the L_α phase (Lindblom et al., 1981; Eriksson & Lindblom, 1993).

One possibility is that the diffusion radius, R, is equivalent to the radius of curvature of the cylinder at the level of the carbonyl segment or unresolved plateau carbons, since the molecules are effectively tethered to the aqueous interface. It is encouraging that the calculated value of $R = 23.7 \pm 5.2$ Å for the H_{II} phase obtained from the excess relaxation rate, $R_{2e}^{HII} - R_{2e}^{L\alpha}$, is rather close to the radius of curvature at the aqueous interface, $R_c = 25.4$ (28.1) Å, deduced from the ^{2}H NMR line shape analysis. Alternatively, if the total transverse relaxation rate in the H_{II} phase, R_{2e}^{HII}, is used for the plateau segments, then the calculated value of the diffusion radius is $R = 32.0 \pm 7.0$ Å, which is in better agreement with the latter value. The above relaxation theory seems to work mainly for carbons in the plateau region of the acyl chains because the model relies on the assumption that the fast and low motions can be separated. Toward the middle and the end of the chains, where the difference in relaxation rates, $R_{2e}^{HII} - R_{2e}^{L\alpha}$, is relatively small, this assumption may no longer hold [cf. Wennerström et al. (1974) and Brown (1982)]. Consequently, we propose that diffusion around the hexagonally packed cylinders may indeed provide a major mechanism for transverse relaxation in these phases. It is also worth noting that, in the normal hexagonal (H_I) phase of potassium laurate-d_{23}, the relaxation enhancement vis-à-vis the lamellar phase (Figure 6) is less than in the case of the H_{II} phase of PLPE-d_{31}. The smaller enhancement for potassium laurate-d_{23} in the H_I phase is consistent with eq 18 because the lateral diffusion coefficients of single-chain amphiphiles in the L_α phase (Roberts, 1973; Lindblom & Wennerström, 1977) are larger than in the case of phospholipids (Lindblom et al., 1976, 1981; Kuo & Wade, 1979). The rather small relaxation enhancement together with the experimental error thus precludes an estimation of the diffusion radius, R. However, one can expect that the radius of curvature, R_c, in the H_I phase aggregates is close to the fully extended chain length as mentioned above.

BIOPHYSICAL CONCLUSIONS

It is increasingly evident that lipids forming nonlamellar phases may exert significant influences on key biological functions involving membrane proteins. Here we have investigated a representative unsaturated phosphatidylethanolamine, PLPE-d_{31}, in the reverse hexagonal (H_{II}) phase in relation to the lamellar, liquid crystalline (L_α) state using deuterium NMR spectroscopy. Significant differences are found in both the deuterium (^{2}H) NMR line shapes and the relaxation rates of PLPE-d_{31} in the various phases which reflect alterations in equilibrium and dynamical properties at the microscopic, viz., the atomic, level. By comparing the ^{2}H NMR order profiles in the reverse hexagonal (H_{II}) and lamellar (L_α) phases one can estimate the *radius of curvature* at the lipid/water interface in the former. The values obtained in this manner are consistent with existing knowledge of the structure of lipid hexagonal phase aggregates and with the interpretation of low-angle X-ray diffraction data for the reverse hexagonal phase of DOPE. Moreover, differences are also found in the transverse relaxation rates (R_{2e}) of the H_{II} and L_α phases of PLPE-d_{31} which yield dynamical information and can also be explained by variations in geometry. We propose that self-diffusion of lipids about the hexagonal phase cylinders provides a mechanism for enhancement of their relaxation rates compared to the planar L_α phase. The calculated diffusion radius in the H_{II} phase is in good agreement with the radius of curvature obtained from analysis of the ^{2}H NMR line shapes. In the future, such investigations can yield a better understanding of the influences of non-bilayer-forming lipids on bilayer properties which may be important in regulation of biological function at the membrane level (Lindblom et al., 1986; Wiedmann et al., 1988; Gibson & Brown, 1993).

ACKNOWLEDGMENT

Many thanks are due to Constantin Job for expert electronics assistance; to Judith Barry for providing some of the computer programs; to Hideo Akutsu, Todd Alam, Ulf Olsson, and Jaroslav Zajicek for helpful discussions; and to Ted Trouard for computer programming and construction of the home-built ^{2}H NMR probe. The comments of a very diligent referee are also gratefully acknowledged.

APPENDIX: RELAXATION DUE TO DIFFUSION ABOUT HEXAGONAL PHASE CYLINDERS

In ^{2}H NMR spectroscopy the relaxation rates typically measured include the following:

$$R_2 = \frac{3}{8}\pi^2\chi^2[3J_0(0) + 3J_1(\omega_0) + 2J_2(2\omega_0)] \qquad (A1a)$$

$$R_{1Z} = \frac{3}{4}\pi^2\chi^2[J_1(\omega_0) + 4J_2(2\omega_0)] \qquad (A1b)$$

$$R_{1Q} = \frac{9}{4}\pi^2\chi^2 J_1(\omega_0) \qquad (A1c)$$

The transverse relaxation rate is designated as R_2, and R_{1Z} and R_{1Q} are the relaxation rates for Zeeman order (spin–lattice relaxation) and quadrupolar order, respectively. Here the static quadrupolar coupling constant is denoted as $\chi \equiv (e^2qQ/h)$, and $\omega_0/2\pi$ is the nuclear Larmor frequency. Note that the relaxation rates depend on the irreducible spectral densities $J_m(m\omega_0)$ in the *laboratory* frame (cf. text), which include the mean-squared amplitudes and rates of the molecular motions (Brown, 1979, 1982).

The result for *diffusion about a single axis* is a limiting case of the more general treatment of anisotropic rotations published earlier (Brown, 1982). In the limit of complete ordering, off-axial fluctuations do not occur. Starting with eqs 2.5 and 3.5 of Brown (1982), in which $\Omega \equiv \Omega_{PM}$, $\Omega' \equiv \Omega_{MD}$, and $\Omega''' \equiv \Omega_{DL}$, we set $\langle D^{(2)}_{00}(\Omega_{MD})\rangle = \langle D^{(4)}_{00}(\Omega_{MD})\rangle = 1$. The Euler angles Ω_{PM} specify rotation of the principal axis system (PAS) of the EFG tensor to the molecular frame; the $\Omega_{MD}(t)$ angles take the latter into the director frame; and finally the angles Ω_{DL} transform the coordinates to the space-fixed (laboratory) frame. The complete ordering leads to collapse of the summation involving $\Omega_{MD} \rightarrow \Omega_{PD}$, yielding in closed form

$$J_m(\omega) = \sum_{n=\pm1,\pm2} |D^{(2)}_{0n}(\Omega_{PD})|^2 |D^{(2)}_{nm}(\Omega_{DL})|^2 j^{(2)}_n(\omega) \quad \text{(A2)}$$

in which

$$j^{(2)}_n(\omega) = \frac{2\tau^{(2)}_n}{1 + \omega^2\tau^{(2)2}_n} \quad \text{(A3)}$$

and the frequency ω is left general ($\omega = m\omega_0$). Here the angles between the C–^{2}H bond direction (PAS of EFG tensor) and the diffusion axis are designated as $\Omega_{PD}(t)$, and axial symmetry of the EFG tensor is assumed. The correlation times are given by $1/\tau^{(2)}_n = n^2D_\parallel$, where $D_\perp$ (=0) and $D_\parallel$ are the principal values of the rotational diffusion tensor $\boldsymbol{D}$. The above formulas correspond to eq 43 of Torchia and Szabo (1982) and eq 72 of Davis (1983) for the case of R_{1Z} due to continuous diffusion (not shown). In eq A2 the products of the Wigner rotation matrix elements are given in closed form by their *Clebsch–Gordan series expansions* (Brink & Satchler, 1968):

$$|D^{(2)}_{m'm}(\Omega)|^2 = (-1)^{m-m'} \sum_j (2j+1) \begin{pmatrix} 2 & 2 & j \\ m' & -m' & 0 \end{pmatrix} \times \begin{pmatrix} 2 & 2 & j \\ m & -m & 0 \end{pmatrix} D^{(j)}_{00}(\Omega) \quad \text{(A4)}$$

Generic Euler angles are denoted by Ω, and the factors in large parentheses indicate *Wigner 3-j symbols*, which couple the rotation matrices of different rank j. The summation over j runs from 0 to 4 in integral steps and is restricted to *even* j values on account of the even parity [cf. Trouard et al. (1992)]. Explicit formulae for the products of the rotation matrix elements are given in eqs 3.7 of Brown (1982). Use of the Clebsch–Gordan series (Brown, 1982) is preferable to formulations in terms of products of trigonometric functions (Torchia & Szabo, 1982; Davis, 1983).

In the case of *hexagonal phase lipids* the motional averaging is divided into two steps, in which *time-scale separation* is assumed [cf. Wennerström et al. (1974) and Brown (1982)]. First, one can average over the faster internal motions of lipids within the aggregate relative to an internal frame (local director), described by the angles $\Omega_{PI}(t)$. This replaces the *static* EFG tensor by an *effective* or *residual* EFG and amounts to simply multiplying the spectral densities in eq A2 by $|\langle D^{(2)}_{00}(\Omega_{PI})\rangle|^2$, which is the fast order parameter squared, viz., $|S^{HH}_{CD}|^2$. Now we consider the slower rotational motion about the cylinder axis, which produces the relaxation. In eq A2 the Euler angles $\Omega_{PD}(t)$ become $\Omega_{IC}(t)$, which transform the coordinates from the internal frame to the major axis of the cylinder, and the angles Ω_{DL} become Ω_{CL}, which rotate the cylinder system to the laboratory frame. With these substitutions, one obtains the general result for diffusion about the cylindrical aggregate from eq A2. We next boldly assume that the internal frame is fixed relative to the cylinder axis at $\Omega_{IC} = (0°, 90°, 0°)$. Substituting $D^{(2)}_{00}(\Omega_{IC}) = -1/2$ and $D^{(4)}_{00}(\Omega_{IC}) = 3/8$ into eq A4 then gives $|D^{(2)}_{0\pm1}(\Omega_{IC})|^2 = 0$ and $|D^{(2)}_{0\pm2}(\Omega_{IC})|^2 = 3/8$. This yields the following result for the spectral densities in the laboratory frame:

$$J_m(\omega) = \frac{3}{4}|\langle D^{(2)}_{00}(\Omega_{PI})\rangle|^2 |D^{(2)}_{2m}(\Omega_{CL})|^2 j^{(2)}_2(\omega) \quad \text{(A5)}$$

in which the dependence of the relaxation on the cylinder orientation relative to the main magnetic field is described by the Euler angles Ω_{CL}. However, the spectral densities can also be averaged over the various orientations with respect to the magnetic field. In the case of isotropic averaging, eq A4 yields $|D^{(2)}_{nm}(\Omega_{CL})|^2 \rightarrow \langle |D^{(2)}_{nm}(\Omega_{CL})|^2\rangle = 1/5$ which become independent of the two projection indices, n and m. This gives $J_m(\omega) \rightarrow \langle J_m(\omega)\rangle \equiv J(\omega)$, leading to the result

$$J(\omega) = \frac{1}{5}|\langle D^{(2)}_{00}(\Omega_{PI})\rangle|^2 \sum_{n=\pm1,\pm2} |D^{(2)}_{0n}(\Omega_{IC})|^2 j^{(2)}_n(\omega) \quad \text{(A6)}$$

Let us now assume that motion about the cylinder axis is too slow to contribute significantly to the $J_1(\omega_0)$ and $J_2(2\omega_0)$ spectral densities (cf. text). The orientationally averaged transverse relaxation rate is obtained from eqs A1a and A6, and assuming $\Omega_{IC} = (0°, 90°, 0°)$ leads to

$$R_2 = \frac{27}{80}\pi^2\chi^2 |\langle D^{(2)}_{00}(\Omega_{PI})\rangle|^2 \tau^{(2)}_2 \quad \text{(A7)}$$

Finally, the correlation times in the above expressions are given by convolution of the spectral densities for surface diffusion of lipids about the cylinder axis with its rotational diffusion described by the coefficient $D_\parallel$ (stochastic equivalence). Following Huntress (1970), the contribution from surface diffusion is obtained by solving (not shown) the *time-dependent diffusion equation* on a cylinder of radius R,

$$\frac{\partial\Psi(\Omega_{IC};t)}{\partial t} = \frac{D_S}{R^2}\hat{\nabla}^2\Psi(\Omega_{IC};t) \quad \text{(A8)}$$

where Ψ is the orientational probability and $\hat{\nabla}^2$ is the Laplacian. This leads to $1/\tau^{(2)}_n = n^2D_S/R^2$, where D_S is the *surface* diffusion coefficient. The effective correlation times for the parallel motion are then given by $1/\tau^{(2)}_n = (D_\parallel + D_S/R^2)n^2$, and provided the surface diffusion is sufficiently rapid, one can neglect $D_\parallel$ as in the text.

REFERENCES

Abdolall, K., Burnell, E. E., & Valic, M. I. (1977) *Chem. Phys. Lipids 20*, 115–129.

Abdolall, K., MacKay, A. L., & Bloom, M. (1978) *J. Magn. Reson. 29*, 309–317.

Abragam, A. (1961) *The Principles of Nuclear Magnetism*, Oxford University Press, Oxford.

Anderson, D., Wennerström, H., & Olsson, U. (1989) *J. Phys. Chem. 93*, 4243–4253.

Barry, J. A., Lamparski, H., Shyamsunder, E., Osterberg, F., Cerne, J., Brown, M. F., & O'Brien, D. F. (1992) *Biochemistry 31*, 10114–10120.
Bechinger, B., Zasloff, M., & Opella, S. J. (1992) *Biophys. J. 62*, 12–14.
Ben-Shaul, A., & Gelbart, W. M. (1985) *Annu. Rev. Phys. Chem. 36*, 179–211.
Bloom, M., & Sternin, E. (1987) *Biochemistry 26*, 2101–2105.
Bloom, M., Burnell, E. E., MacKay, A. L., Nichol, C. P., Valic, M. I., & Weeks, G. (1978) *Biochemistry 17*, 5750–5762.
Bloom, M., Davis, J. H., & Valic, M. I. (1980) *Can. J. Phys. 58*, 1510–1517.
Bloom, M., Davis, J. H., & MacKay, A. L. (1981) *Chem. Phys. Lett. 80*, 198–202.
Bocian, D. F., & Chan, S. I. (1978) *Annu. Rev. Phys. Chem. 29*, 307–335.
Bolen, E. J., & Sando, J. J. (1992) *Biochemistry 31*, 5945–5951.
Bonmatin, J.-M., Smith, I. C. P., Jarrell, H. C., & Siminovitch, D. J. (1988) *J. Am. Chem. Soc. 110*, 8693–8695.
Bonmatin, J.-M., Smith, I. C. P., Jarrell, H. C., & Siminovitch, D. J. (1990) *J. Am. Chem. Soc. 112*, 1697–1704.
Brink, D. M., & Satchler, G. R. (1968) *Angular Momentum*, Oxford University Press, Oxford.
Brown, M. F. (1979) *J. Magn. Reson. 35*, 203–215.
Brown, M. F. (1982) *J. Chem Phys. 77*, 1576–1598.
Brown, M. F. (1990) *Mol. Phys. 71*, 903–908.
Brown, M. F., & Davis, J. H. (1981) *Chem. Phys. Lett. 79*, 431–435.
Brown, M. F., & Söderman, O. (1990) *Chem. Phys. Lett. 167*, 158–164.
Brown, M. F., & Gibson, N. J. (1992) in *Essential Fatty Acids and Eicosanoids* (Sinclair, A., & Gibson, R., Eds.) pp 134–138, AOCS Press, Champaign, IL.
Büldt, G., Gally, H. U., Seelig, J., & Zaccai, G. (1979) *J. Mol. Biol. 134*, 673–691.
Comfurius, P., & Zwaal, R. F. A. (1977) *Biochim. Biophys. Acta 488*, 36–42.
Cullis, P. R., & de Kruijff, B. (1978) *Biochim. Biophys. Acta 513*, 31–42.
Cullis, P. R., & de Kruijff, B. (1979) *Biochim. Biophys. Acta 559*, 399–420.
Davis, J. H. (1979) *Biophys. J. 27*, 339–359.
Davis, J. H. (1983) *Biochim. Biophys. Acta 737*, 117–171.
Davis, J. H., Jeffrey, K. R., Bloom, M., Valic, M. I., & Higgs, T. P. (1976) *Chem. Phys. Lett. 42*, 390–394.
Deese, A. J., Dratz, E. A., & Brown, M. F. (1981) *FEBS Lett. 124*, 93–99.
DeYoung, L. R., & Dill, K. A. (1988) *Biochemistry 27*, 5281–5289.
Dill, K. A., & Flory, P. J. (1980) *Proc. Natl. Acad. Sci. U.S.A. 77*, 3115–3119.
Dill, K. A., Naghizadeh, J., & Marqusee, J. A. (1988) *Annu. Rev. Phys. Chem. 39*, 425–461.
Dodd, S. W. (1987) M.S. Thesis, University of Virginia.
Ekwall, P. (1975) *Adv. Liq. Cryst. 1*, 1–142.
Ellena, J. F., Pates, R. D., & Brown, M. F. (1986) *Biochemistry 25*, 3742–3748.
Epand, R. M. (1992) in *Protein Kinase C Current Concepts and Future Perspectives* (Lester, D. S., & Epand, R. M., Eds.) Simon & Schuster, Herts, England (in press).
Eriksson, P.-O., & Lindblom, G. (1993) *Biophys. J. 64*, 129–136.
Eriksson, P.-O., Khan, A., & Lindblom, G. (1982) *J. Phys. Chem. 86*, 387–393.
Eriksson, P.-O., Lindblom, G., & Arvidson, G. (1987) *J. Phys. Chem. 91*, 846–853.
Eriksson, P.-O., Rilfors, L., Wieslander, Å., Lundberg, A., & Lindblom, G. (1991) *Biochemistry 30*, 4916–4924.
Fuson, M. M., & Prestegard, J. H. (1983a) *J. Am. Chem. Soc. 105*, 168–176.
Fuson, M. M., & Prestegard, J. H. (1983b) *Biochemistry 22*, 1311–1316.
Gibson, N. J., & Brown, M. F. (1991) *Photochem. Photobiol. 54*, 985–992.
Gibson, N. J., & Brown, M. F. (1993) *Biochemistry 32*, 2438–2454.
Griffin, R. G. (1981) *Methods Enzymol. 72*, 108–174.
Gruen, D. W. R. (1980) *Biochim. Biophys. Acta 595*, 161–183.
Gruen, D. W. R. (1985) *J. Phys. Chem. 89*, 153–163.
Gruner, S. M. (1989) *J. Phys. Chem. 93*, 7562–7570.
Gruner, S. M., Parsegian, V. A., & Rand, R. P. (1986) *Faraday Discuss. Chem. Soc. 81*, 29–37.
Halle, B. (1987) *Mol. Phys. 61*, 963–980.
Halle, B. (1991) *J. Phys. Chem. 95*, 6724–6733.
Helfrich, W. (1973) *Z. Naturforsch. C 28*, 693–703.
Henriksson, U., Ödberg, L., & Eriksson, J. C. (1975) *Mol. Cryst. Liq. Cryst. 30*, 73–78.
Higgs, T. P., & MacKay, A. L. (1977) *Chem. Phys. Lipids 20*, 105–114.
Huang, C.-h. (1969) *Biochemistry 8*, 344–351.
Huntress, W. T., Jr. (1970) *Adv. Magn. Reson. 4*, 1–37.
Ipsen, J. H., Mouritsen, O. G., & Bloom, M. (1990) *Biophys. J. 57*, 405–412.
Israelachvili, J. N., Mitchell, D. J., & Ninham, B. W. (1976) *J. Chem. Soc., Faraday Trans. 2 72*, 1525–1568.
Jansson, M., Thurmond, R. L., Trouard, T. P., & Brown, M. F. (1990) *Chem. Phys. Lipids 54*, 157–170.
Jansson, M., Thurmond, R. L., Barry, J. A., & Brown, M. F. (1992) *J. Phys. Chem. 96*, 9532–9544.
Jarrell, H. C., Smith, I. C. P., Jovall, P. A., Mantsch, H. H., & Siminovitch, D. J. (1988) *J. Chem. Phys. 88*, 1260–1263.
Jeffrey, K. R., Wong, T. C., & Tulloch, A. P. (1984) *Mol. Phys. 52*, 289–306.
Jensen, J. W., & Schutzbach, J. S. (1984) *Biochemistry 23*, 1115–1119.
Jensen, J. W., & Schutzbach, J. S. (1988) *Biochemistry 27*, 6315–6320.
Jensen, R. G., & Pitas, R. E. (1976) *Adv. Lipid Res. 14*, 213–247.
Jonas, J., Winter, R., Grandinetti, P. J., & Driscoll, D. (1990) *J. Magn. Reson. 87*, 536–547.
Kaufmann, S., Wefing, S., Schaefer, D., & Spiess, H. W. (1990) *J. Chem. Phys. 93*, 197–214.
Kintanar, A., Kunwar, A. C., & Oldfield, E. (1986) *Biochemistry 25*, 6517–6524.
Kirk, G. L., Gruner, S. M., & Stein, D. L. (1984) *Biochemistry 23*, 1093–1102.
Korstanje, L. J., van Faassen, E. E., & Levine, Y. K. (1989) *Biochim. Biophys. Acta 982*, 196–204.
Kuo, A.-L., & Wade, C. G. (1979) *Biochemistry 18*, 2300–2308.
Lafleur, M., Cullis, P., Fine, B., & Bloom, M. (1990) *Biochemistry 29*, 8325–8333.
Lepore, L. S., Ellena, J. F., & Cafiso, D. S. (1992) *Biophys. J. 61*, 767–775.
Lindblom, G., & Wennerström, H. (1977) *Biophys. Chem. 6*, 167–171.
Lindblom, G., & Rilfors, L. (1989) *Biochim. Biophys. Acta 998*, 221–256.
Lindblom, G., Wennerström, H., Arvidson, G., & Lindman, B. (1976) *Biophys. J. 16*, 1287–1295.
Lindblom, G., Johansson, L. B.-Å., & Arvidson, G. (1981) *Biochemistry 20*, 2204–2207.
Lindblom, G., Brentel, I., Sjölund, M., Wikander, G., & Wieslander, Å. (1986) *Biochemistry 25*, 7502–7510.
Luzzati, V. (1968) in *Biological Membranes Vol. 1* (Chapman, D., Ed.) pp 71–123, Academic Press, New York.
Mason, J. T., Broccoli, A. V., & Huang, C.-h. (1981) *Anal. Biochem. 113*, 96–101.
Mayer, C., Gröbner, G., Müller, K., Weisz, K., & Kothe, G. (1990) *Chem. Phys. Lett. 165*, 155–161.
Meraldi, J.-P., & Schlitter, J. (1981) *Biochim. Biophys. Acta 645*, 183–192.
Nagle, J. F. (1975) *J. Chem. Phys. 63*, 1255–1261.
Nagle, J. F., & Wilkinson, D. A. (1978) *Biophys. J. 23*, 159–175.

Nagle, J. F., & Wiener, M. C. (1988) *Biochim. Biophys. Acta 942*, 1–10.
Navarro, J., Toivio-Kinnucan, M., & Racker, E. (1984) *Biochemistry 23*, 130–135.
Opella, S. J., Stewart, P. L., & Valentine, K. G. (1987) *Q. Rev. Biophys. 19*, 7–49.
Orädd, G., Lindblom, G., Johansson, L. B.-Å., & Wikander, G. (1992) *J. Phys. Chem. 96*, 5170–5174.
Parmar, Y. I., Wassall, S. R., & Cushley, R. J. (1984) *J. Am. Chem. Soc. 106*, 2434–2435.
Rance, M., & Byrd, R. A. (1983) *J. Magn. Reson. 52*, 221–240.
Rand, R. P., Fuller, N. L., Gruner, S. M., & Persegian, V. A. (1990) *Biochemistry 29*, 76–87.
Rilfors, L., Lindblom, G., Wieslander, Å., & Christiansson, A. (1984) *Biomembranes 12*, 205–237.
Roberts, R. T. (1973) *Nature (London) 242*, 348.
Rossini, F. D., Pitzer, K. S., Arnett, R. L., Braun, R. M., & Pimentel, G. C. (1953) *Selected Values of Physical Properties of Hydrocarbons and Related Compounds*, Carnegie Press, Pittsburg.
Salmon, A., Dodd, S. W., Williams, G. D., Beach, J. M., & Brown, M. F. (1987) *J. Am. Chem. Soc. 109*, 2600–2609.
Schindler, H., & Seelig, J. (1975) *Biochemistry 14*, 2283–2287.
Seddon, J. M. (1990) *Biochim. Biophys. Acta 1031*, 1–69.
Seelig, J. (1977) *Q. Rev. Biophys. 10*, 353–418.
Seelig, J. (1978) *Biochim. Biophys. Acta 515*, 105–140.
Seiter, C. H. A., & Chan, S. I. (1973) *J. Am. Chem. Soc. 95*, 7541–7553.
Shipley, G. G. (1968) in *Biological Membranes Vol. 1* (Chapman, D., Ed.) pp 1–89, Academic Press, New York.
Sjölund, M., Lindblom, G., Rilfors, L., & Arvidson, G. (1987) *Biophys. J. 52*, 145–153.
Small, D. M. (1986) *The Physical Chemistry of Lipids*, Plenum Press, New York.
Söderman, O., Henriksson, U., & Olsson, U. (1987) *J. Phys. Chem. 91*, 116–120.
Söderman, O., Carlström, G., Olsson, U., & Wong, T. C. (1988) *J. Chem. Soc., Faraday Trans. 1 84*, 4475–4486.
Söderman, O., Ginley, M., Henriksson, U., Malmvik, A.-C., & Johansson, L. B.-Å. (1990) *J. Chem. Soc., Faraday Trans. 86*, 1555–1559.
Speyer, J. B., Weber, R. T., Das Gupta, S. K., & Griffin, R. G. (1989) *Biochemistry 28*, 9569–9574.
Sternin, E., Bloom, M., & MacKay, A. L. (1983) *J. Magn. Reson. 55*, 274–282.
Sternin, E., Fine, B., Bloom, M., Tilcock, C. P. S., Wong, K. F., & Cullis, P. R. (1988) *Biophys. J. 54*, 689–694.
Stockton, G. W., Polnaszek, C. F., Tulloch, A. P., Hasan, F., & Smith, I. C. P. (1976) *Biochemistry 15*, 954–966.
Stohrer, J., Gröbner, G., Reimer, D., Weisz, K., Mayer, C., & Kothe, G. (1991) *J. Chem. Phys. 95*, 672–678.
Tanford, C. (1980) *The Hydrophobic Effect*, Wiley, New York.
Tardieu, A., Luzzati, V., & Reman, F. C. (1973) *J. Mol. Biol. 75*, 711–733.
Tartar, H. V. (1955) *J. Phys. Chem. 59*, 1195–1199.
Tate, M. W., & Gruner, S. M. (1989) *Biochemistry 28*, 4245–4253.
Thurmond, R. L., Lindblom, G., & Brown, M. F. (1990) *Biochem. Biophys. Res. Commun. 173*, 1231–1238.
Thurmond, R. L., Dodd, S. W., & Brown, M. F. (1991) *Biophys. J. 59*, 108–113.
Torchia, D. A., & Szabo, A. (1982) *J. Magn. Reson. 49*, 107–121.
Trouard, T. P., Alam, T. M., Zajicek, J., & Brown, M. F. (1992) *Chem. Phys. Lett. 189*, 67–75.
Wennerström, H., & Lindblom, G. (1977) *Q. Rev. Biophys. 10*, 67–96.
Wennerström, H., Lindblom, G., & Lindman, B. (1974) *Chem. Scr. 6*, 97–103.
Wennerström, H., Lindman, B., Söderman, O., Drakenberg, T., & Rosenholm, J. B. (1979) *J. Am. Chem. Soc. 101*, 6860–6864.
Wiedmann, T. S., Pates, R. D., Beach, J. M., Salmon, A., & Brown, M. F. (1988) *Biochemistry 27*, 6469–6474.
Wiener, M. C., & White, S. H. (1992) *Biophys. J. 61*, 434–447.
Wiener, M. C., Tristram-Nagle, S., Wilkinson, D. A., Campbell, L. E., & Nagle, J. F. (1988) *Biochim. Biophys. Acta 938*, 135–142.
Wiener, M. C., King, G. I., & White, S. H. (1991) *Biophys. J. 60*, 568–576.
Wilkinson, D. A., & Nagle, J. F. (1981) *Biochemistry 20*, 187–192.
Williams, G. D., Beach, J. M., Dodd, S. W., & Brown, M. F. (1985) *J. Am. Chem. Soc. 107*, 6868–6873.
Xu, Z.-C., & Cafiso, D. S. (1986) *Biophys. J. 49*, 779–783.
Yang, S. F., Freer, S., & Benson, A. A. (1967) *J. Biol. Chem. 242*, 477–484.